4. Iron Isotope Fractionation by Fe(II)-oxidizing Photoautotrophic Bacteria

ABSTRACT

Photoautotrophic bacteria that oxidize ferrous iron [Fe(II)] under anaerobic conditions are thought to be ancient in origin, and the ferric (hydr)oxide mineral products of their metabolism are likely to be preserved in ancient rocks. Here, two enrichment cultures of Fe(II)-oxidizing photoautotrophs and a culture of the genus *Thiodictyon* were studied with respect to their ability to fractionate Fe isotopes. Fe isotope fractionations produced by both the enrichment cultures and the *Thiodictyon* culture were relatively constant at early stages of the reaction progress, where the $^{56}Fe\,/^{54}Fe$ ratios of poorly crystalline hydrous ferric oxide (HFO) metabolic products were enriched in the heavier isotope relative to aqueous ferrous iron ($Fe(II)_{aq}$) by ~1.5±0.2 per mil (‰). This fractionation appears to be independent of the rate of photoautotrophic Fe(II)-oxidation, and is comparable to that observed for Fe isotope fractionation by dissimilatory Fe(III)-reducing bacteria. Although there remain a number of uncertainties regarding how the overall measured isotopic fractionation is produced, the most likely mechanisms include 1) an equilibrium effect produced by biological ligands, or 2) a kinetic effect produced by precipitation of HFO overlaid upon equilibrium exchange between Fe(II) and Fe(III) species. The fractionation we observe is similar in direction to that measured for abiotic oxidation of $Fe(II)_{aq}$ by molecular

oxygen. This suggests that the use of Fe isotopes to identify phototrophic Fe(II)-oxidation in the rock record may only be possible during time periods in Earth's history when independent evidence exists for low ambient oxygen contents.

INTRODUCTION

Geochemical cycling of iron (Fe) is primarily controlled by redox conditions, which vary markedly in different environments on the modern Earth, and have likely changed over geologic time. It is widely (though not universally) accepted that the terrestrial atmosphere has been oxidizing for at least the last two billion years [58, 74, 91, 106, 128, 145]. As a result, chemical oxidation of ferrous iron [Fe(II)] under "modern" atmospheric conditions often occurs through the interaction of reduced fluids with oxygenated waters. An important exception to this, however, is Fe(II)-oxidation that occurs in microaerobic or anoxic environments as a result of the activity of microorganisms that oxidize Fe(II) to generate energy for growth. Microorganisms of this type include those that couple Fe(II)-oxidation to the reduction of nitrate at neutral pH [14, 162], or to the reduction of oxygen at either low [18, 50], or neutral pH [54], and the anaerobic Fe(II)-oxidizing phototrophs [52, 70, 182]. Under oxygen-deplete conditions, microbially mediated Fe(II)-oxidation is an important component of the Fe redox cycle.

In most cases, the products of biologically oxidized Fe are highly insoluble ferric [Fe(III)] (hydr)oxide minerals that are likely to be preserved in rocks. Indeed, direct photoautotrophic Fe(II)-oxidation under anaerobic conditions (as

opposed to indirect photoautotrophic Fe(II)-oxidation mediated by oxygen produced by cyanobacteria [37]), has been proposed as a mechanism for producing the extensive ferric oxide deposits found in ancient Banded Iron Formations (BIFs) [67, 101, 182]. Therefore, studies of the mechanisms of direct biological Fe(II)-oxidation and the structure and composition of the resulting Fe(III) mineral products may be useful in furthering our understanding of the geochemical cycling of Fe that occurred on the ancient Earth. To evaluate the role of microbes in Fe cycling today and over geological time, however, we are faced with the challenge of distinguishing between Fe(III) minerals that formed via biological or abiotic pathways.

It has been suggested that Fe isotope geochemistry may be useful in such a context [10], and a number of measurements of Fe isotope fractionation have been made in biological [10, 11, 22, 85, 116], and abiotic [4, 10-12, 27, 86, 117, 141, 155, 181] experimental systems. Although most igneous rocks and many clastic sedimentary materials are isotopically homogeneous within ±0.05‰ [11], significant variations (~ 4‰) in Fe isotope compositions are found in late Archean BIFs [84].

If Fe isotopes are to be used to broaden our understanding of the Fe cycle, and the isotopic variations observed in BIFs, a better understanding of the Fe isotope fractionations that are produced by abiotic and biological transformations of Fe is needed. In particular, biological redox processes that alter the oxidation state of Fe are of interest because Fe isotopic fractionations in low temperature natural systems are predicted to be greatest between Fe(II) and

Fe(III) phases [146]. Although Fe isotope fractionations produced during dissimilatory Fe(III)-reduction by *Shewanella alga* have been measured [10, 11], no data currently exist to constrain Fe isotope fractionations that may occur during microbial Fe(II)-oxidation.

To make inferences about Fe cycling on the ancient Earth using Fe isotopes, it is important to study Fe(II)-oxidizing organisms that carry out an ancient form of metabolism. The use of Fe(II) as an electron donor in anoxygenic photosynthesis likely arose early in Earth history. This assumption rests on the fact that phylogenetic relationships between genes that are involved in bacteriochlorophyll and chlorophyll biosynthesis show that the anoxygenic form of photosynthesis evolved before the oxygenic form [185], as well as the logic that the evolution of oxygenic photosynthesis predates the evolution of respiratory metabolisms that are based on oxygen or other highly oxidized species (*i.e.*, nitrate). In addition, the high estimated concentrations of reduced Fe that appear to have existed in the early Earth's oceans relative to today [57, 72, 184], suggest that Fe(II) was available to fuel microbial metabolism early in Earth history. Therefore, this study focuses on Fe isotope fractionation produced by anoxygenic Fe(II)-oxidizing photoautotrophic bacteria, as opposed to other Fe(II)-oxidizing bacteria.

EXPERIMENTAL PROCEDURES

Organisms and cultivation

Two enrichment cultures of Fe(II)-oxidizing anoxygenic phototrophs were obtained from an Fe-rich ditch in Bremen, Germany. The Fe(II)-oxidizing phototroph, strain F4, was isolated from a marsh in Woods Hole, MA

For routine cultivation, all cultures were maintained in an anoxic minimal salts medium for freshwater cultures [52]. One liter (L) of medium contained: 0.3 grams (g) NH_4Cl, 0.5 g KH_2PO_4, 0.4 g $MgCl_2 \cdot 6H_2O$, 0.1 g $CaCl_2 \cdot 2H_2O$. After sterilization by autoclaving, the basal salts solution was equilibrated with a 20% CO_2:80% N_2 gas mix. Additions to the cooled medium included: 22 milliliters (ml) 1 Molar (M) $NaHCO_3$, 1 ml of a trace elements solution (3 g Na_2-EDTA, 1.1 g $FeSO_4 \cdot 7H_2O$, 190 mg $CoCl_2 \cdot 6H_2O$, 42 mg $ZnCl_2$, 24 mg $NiCl_2 \cdot 6 H_2O$, 18 mg $Na_2MoO_4 \cdot 2H_2O$, 300 mg H_3BO_3, 2 mg $CuCl_2 \cdot 2H_2O$ and 50 mg $MnCl_2 \cdot 4H_2O$ in 1 L ultra-pure $H2O$), 1 ml of a vitamin solution (4 mg 4-aminobenzoic acid, 1 mg D(+)-biotin, 10 mg nicotinic acid, 5 mg Ca D(+)-pantothenate, 15 mg pyridoxine dihydrochloride, and 10 mg thiamine chloride dihydrochloride in 1 L ultra-pure H_2O), and 1 ml of a vitamin B_{12} solution (5 mg in 50 ml ultra-pure H_2O). The medium was adjusted to pH 7 with 1 M HCl.

Fe(II) additions to the basal medium were made in an anaerobic chamber (Coy Laboratory Products, Grasslake, MI). 10 ml of an anoxic, 1 M $FeCl_2 \cdot H_2O$ stock solution was added to the medium batch used to grow the enrichments, whereas 15 ml was added to the batch used to grow strain F4. Upon addition of Fe(II) to the medium, a fluffy white precipitate, most likely vivianite ($Fe_3(PO_4)$

$_2 \cdot 8H_2O$) or a vivianite and siderite (FeCO$_3$) mixture, formed. To eliminate this precipitate from Fe(III) precipitates that would later be produced during biological Fe(II)-oxidation, precipitation was allowed to proceed for approximately 14-18 hours, after which all precipitates were filtered out (0.2 μm, cellulose nitrate, Millipore), leaving a clear medium with ~6-10 mM Fe(II)$_{aq}$. Filtration was performed in the anaerobic chamber. Twenty-five ml aliquots of the Fe(II)-containing medium were dispensed anaerobically into 58 ml serum bottles, stoppered and maintained under a 20% CO$_2$:80% N$_2$ gas atmosphere. Most cultures were incubated at a distance of 40 cm from a 40 Watt (W) standard incandescent light source at 22°C, except for those incubated at 80 and 120 cm distances; all were gently inverted daily to mix the cultures.

The ferrous precipitates were ~0.3‰ heavier in ^{56}Fe $/^{54}$Fe ratios than the starting 1 M FeCl$_2 \cdot$H$_2$O stock solutions, producing a medium supernatant that was lower in δ^{56}Fe values than the starting FeCl$_2 \cdot$H$_2$O reagent (Table 4-1). The fact that the δ^{56}Fe values in the aqueous fractions of the uninoculated controls for the microbial experiments were different from the controls listed in the Table 4-1 is surprising, but may be explained by differences in timing of medium sampling (*i.e.*, we sampled our reagent controls after only 2-3 hours, and it is probable that not all of the ferrous solids had precipitated by this point, whereas ferrous solid precipitation appears to have been complete in the medium used for the microbial experiments). Note that the solid FeCl$_2 \cdot$H$_2$O reagent is isotopically heterogeneous on the ~100 μg scale (Table 4-1), although this scale of isotopic

heterogeneity is homogenized by the large amounts of solid used in the $FeCl_2 \cdot H_2O$ regent preparation.

Table 4-1: Fe isotope compositions of the experimental reagents and enrichment culture inoculums. In the analyses column, up to triplicate mass spectrometry runs of a sample conducted on different days are reported; the errors are 2-SE from in-run statistics and reflect machine uncertainties and/or processing errors. The Mass Spec Average is the average of up to three analyses of a single sample, 1-SD is one standard deviation external; note that if there is only one mass spectrometry analysis, the error is 2-SE. The Average of Replicate is the average of processing replicates of a sample throughout the entire analytical procedure; the best estimate of external reproducibility. [1]Inoculum refers to the cells and small amount of Fe(III) precipitates (~1.2 millimoles) transferred from a grown culture of the enrichments to the fresh filtered Fe(II) medium used for these experiments. Inoculum cultures where the Fe(II) substrate initially provided was oxidized to completion were used to minimize Fe carryover. [2]Yellow crystals among the bulk of the green crystals of the solid $FeCl_2 \cdot H_2O$ used for the isotopic experiments indicate slight oxidation of the reagent. The isotopic composition of the solid $FeCl_2 \cdot H_2O$ reagent is heterogeneous on the 100 mg scale. [3]1M $FeCl_2 \cdot H_2O$ stock solution used for enrichment medium preparation. [4]10 mM $FeCl_2 \cdot H_2O$ was added to 25 mls of medium. The resulting ferrous minerals were allowed to precipitate to completion. Under an aerobic atmosphere, the medium was mixed well and 1 ml

was extracted with a syringe and transferred to a microcentrifuge tube. The precipitate and soluble phases were separated by centrifugation. The soluble phase was removed with a pipette and filtered through a 0.22 µm filter into a clean microcentrifuge tube. The precipitate fraction was washed three times with ultra pure water equilibrated with an anoxic atmosphere. Supernatant 1, 2 and 3 are triplicate samples of the soluble phase and precipitate 1 and 2 are duplicate samples of the precipitate phase.

Table 4-1:

Sample	Analyses				Mass Spec Average				Average of Replicates			
	$\delta^{56}Fe$	2-SE	$\delta^{56}Fe$	2-SE	$\delta^{56}Fe$	1-SD	$\delta^{56}Fe$	1-SD	$\delta^{56}Fe$	1-SD	$\delta^{56}Fe$	1-SD
Inoculum for enrichment culture 1[1]	-0.31	0.06	-0.48	0.03	-0.31	0.01	-0.46	0.02	---	---	---	---
	-0.31	0.08	-0.45	0.04								
Inoculum for enrichment culture 2[1]	-0.35	0.06	-0.55	0.04	---	---	---	---	---	---	---	---
0.36 mg of $FeCl_2 \cdot H_2O$ salt crystals	-0.04	0.06	0.08	0.04	-0.06	0.03	-0.03	0.15	---	---	---	---
	-0.08	0.13	-0.13	0.06								
0.38 mg of green $FeCl_2 \cdot H_2O$ salt crystals[2]	-0.41	0.14	-0.68	0.06	-0.48	0.09	-0.68	0.06	---	---	---	---
	-0.45	0.06	-0.62	0.03								
	-0.57	0.08	-0.75	0.04								
0.44 mg of green $FeCl_2 \cdot H_2O$ salt crystals[2]	-0.13	0.06	-0.17	0.03	-0.14	0.02	-0.21	0.06	---	---	---	---
	-0.16	0.09	-0.25	0.04								
0.35 mg of yellow $FeCl_2 \cdot H_2O$ salt crystals[2]	-0.22	0.12	-0.33	0.07	-0.25	0.09	-0.42	0.15	---	---	---	---
	-0.36	0.06	-0.59	0.03								
	-0.19	0.07	-0.34	0.04								
0.47 mg of yellow $FeCl_2 \cdot H_2O$ salt crystals[2]	-0.11	0.13	-0.09	0.06	-0.07	0.12	-0.08	0.22	---	---	---	---
	0.07	0.05	0.14	0.05								
	-0.16	0.07	-0.30	0.03								
~200mg of $FeCl_2 \cdot H_2O$ salt crystals dissolved into a 400 ppm Fe solution	-0.41	0.11	-0.48	0.06	-0.37	0.04	-0.46	0.09	---	---	---	---
	-0.33	0.07	-0.36	0.04								
	-0.36	0.07	-0.53	0.03								

1 M FeCl$_2$·H$_2$O stock solutions – 1[3]	-0.42	0.07	-0.53	0.04	---	---	---	---	-0.36	0.03	-0.51	0.01
1 M FeCl$_2$·H$_2$O stock solutions – 2[3]	-0.36	0.08	-0.55	0.04	-0.32	0.05	-0.50	0.08	---	---	---	---
	-0.29	0.12	-0.45	0.06								
Supernatant 1[4]	-0.63	0.09	-1.03	0.04	-0.72	0.10	-1.14	0.11	-0.70	0.09	-1.09	0.12
	-0.84	0.09	-1.25	0.05								
	-0.71	0.09	-1.15	0.04								
Supernatant 2[4]	-0.69	0.08	-1.02	0.10	-0.68	0.10	-1.04	0.11	---	---	---	---
	-0.78	0.05	-1.15	0.04								
	-0.59	0.08	-0.94	0.04								
Supernatant 3[4]	-0.69	0.10	-0.94	0.05	-0.77	0.11	-1.08	0.19	---	---	---	---
	-0.85	0.07	-1.21	0.04								
Precipitate 1[4]	-0.07	0.13	-0.12	0.06	-0.11	0.05	-0.18	0.06	-0.08	0.05	-0.12	0.11
	-0.16	0.08	-0.22	0.06								
	-0.09	0.12	-0.22	0.05								
Precipitate 2[4]	-0.04	0.09	-0.08	0.06	-0.05	0.02	-0.06	0.12	---	---	---	---
	-0.04	0.10	0.06	0.06								
	-0.07	0.12	-0.17	0.06								

After filtration, no further precipitation of Fe(II) minerals was observed in uninoculated controls or in inoculated dark controls throughout the course of the experiments. This can be seen in Tables 4-2 and 3, which show invariant Fe(II) concentrations and Fe isotope compositions of the uninoculated controls, as well as the inoculated control that was incubated in the dark. Therefore, the current study avoids ambiguities in interpreting isotopic data that have been encountered by other researchers due to the simultaneous precipitation of Fe(II) and Fe(III) mineral phases during Fe(II)-oxidation [108].

Table 4-2: Fe isotope compositions of enrichments 1 and 2 and the uninoculated control. All cultures started at 25 ml total volume. Sampling volumes were always 1 ml, and were split into two 0.5 ml sub-volumes to obtain duplicate soluble and precipitate (ppt) fractions for that time point. Start volume is the volume of the culture on the day the sample was taken. Mmol Fe(III) is calculated by mass balance using the *Ferrozine* measurements for Fe(II). "*F*" represents the fraction of the total Fe(II)$_{aq}$ that has been oxidized. In the analyses column, up to triplicate mass spectrometry runs of a sample conducted on different days are reported; the errors are 2-SE from in-run statistics and reflect machine uncertainties and/or processing errors. The Mass Spec Average is the average of up to three analyses of a single sample, 1-SD is one standard deviation external; note that if there is only one mass spectrometry analysis, the error is 2-SE. The Average of Replicate is the average of processing replicates

of a sample throughout the entire analytical procedure; the best estimate of

external reproducibility. [1]per 0.5 ml split

Table 4-2:

Sample/ Day/ Start Volume (ml)	Fe(II) mmol[1]	Fe(III) mmol[1]	F	Analyses				Mass Spec Average				Average of Replicates			
				$\delta^{56}Fe$	2-SE	$\delta^{57}Fe$	2-SE	$\delta^{56}Fe$	1-SD	$\delta^{57}Fe$	1-SD	$\delta^{56}Fe$	1-SD	$\delta^{57}Fe$	1-SD
Enrichment 1															
Soluble fraction 1/0/25	2.75	---	0.000	-0.40	0.07	-0.53	0.03	---	---	---	---	-0.40	0.07	-0.53	0.03
Soluble fraction 2/0/25	2.75	---	0.000	-0.41	0.07	-0.57	0.03	-0.46	0.07	-0.64	0.10				
				-0.51	0.08	-0.71	0.05								
Soluble fraction 1/3/24	2.94	---	0.000	-0.42	0.07	-0.65	0.04	-0.42	0.01	-0.66	0.02	-0.42	0.01	-0.62	0.05
				-0.42	0.06	-0.67	0.03								
Soluble fraction 2/3/24	2.94	---	0.000	-0.43	0.06	-0.56	0.03	-0.42	0.01	-0.58	0.02				
				-0.42	0.06	-0.59	0.03								
Soluble fraction 1/9/23	2.56	---	0.068	-0.71	0.07	-1.03	0.03	-0.69	0.03	-1.02	0.01	-0.77	0.14	-1.11	0.16
				-0.67	0.06	-1.02	0.03								
Soluble fraction 2/9/23	2.56	---	0.068	-0.93	0.05	-1.30	0.03	---	---	---	---				
Soluble fraction 1/11/22	0.55	---	0.801	-2.21	0.06	-3.17	0.03	-2.22	0.01	-3.17	0.00	-2.23	0.02	-3.22	0.06
				-2.22	0.11	-3.17	0.05								
Soluble fraction 2/11/22	0.55	---	0.801	-2.27	0.07	-3.28	0.04	-2.25	0.02	-3.27	0.01				
				-2.24	0.09	-3.27	0.04								
Soluble fraction 1/13/21	0.25	---	0.909	---	---	---	---	---	---	---	---	---	---	---	---
Soluble	0.25	---	0.909	---	---	---	---	---	---	---	---				

fraction 2/13/21															
Ppt. fraction 1/0/25	---	0.00	0.000	---	---	---	---	---	---	---	---	---	---	---	---
Ppt. fraction 2/0/25	---	0.00	0.000	---	---	---	---	---	---	---	---				
Ppt. fraction 1/3/24	---	0.00	0.000	---	---	---	---	---	---	---	---	---	---	---	---
Ppt. fraction 2/3/24	---	0.00	0.000	---	---	---	---	---	---	---	---				
Ppt. fraction 1/9/23	---	0.19	0.068	0.85	0.07	1.22	0.04	0.82	0.04	1.20	0.03	---	---	---	---
				0.80	0.06	1.18	0.04								
Ppt. fraction 2/9/23	---	0.19	0.068	---	---	---	---	---	---	---	---				
Ppt. fraction 1/11/22	---	2.20	0.801	0.01	0.07	-0.01	0.03	-0.01	0.02	0.01	0.02	-0.03	0.05	-0.02	0.04
				-0.03	0.06	0.02	0.04								
Ppt. fraction 2/11/22	---	2.20	0.801	-0.08	0.07	-0.07	0.03	---	---	---	---				
Ppt. fraction 1/13/21	---	2.50	0.909	-0.28	0.08	-0.40	0.04	---	---	---	---	-0.20	0.07	-0.29	0.07
Ppt. fraction 2/13/21	---	2.50	0.909	-0.10	0.07	-0.26	0.05	-0.17	0.06	-0.26	0.02				
				-0.19	0.06	-0.23	0.03								
				-0.22	0.07	-0.28	0.04								
Enrichment 2															
Soluble fraction 1/0/25	2.98	---	0.000	-0.41	0.08	-0.56	0.05	-0.43	0.03	-0.60	0.06	-0.43	0.03	-0.61	0.06
				-0.45	0.05	-0.65	0.03								

Soluble fraction 2/0/25	2.98	---	0.000	-0.40	0.13	-0.57	0.06	-0.42	0.03	-0.62	0.08				
				-0.45	0.06	-0.68	0.03								
Soluble fraction 1/3/24	2.59	---	0.131	-0.35	0.08	-0.62	0.04	-0.38	0.04	-0.60	0.02	-0.43	0.06	-0.64	0.06
				-0.41	0.06	-0.59	0.03								
Soluble fraction 2/3/24	2.59	---	0.131	-0.47	0.08	-0.65	0.18	-0.48	0.02	-0.68	0.05				
				-0.49	0.08	-0.72	0.04								
Soluble fraction 1/9/23	2.20	---	0.264	-0.87	0.08	-1.26	0.05	-0.88	0.01	-1.24	0.04	-0.86	0.04	-1.21	0.04
				-0.89	0.07	-1.21	0.04								
Soluble fraction 2/9/23	2.20	---	0.264	-0.80	0.09	-1.17	0.04	-0.84	0.05	-1.19	0.03				
				-0.88	0.09	-1.21	0.05								
Soluble fraction 1/11/22	1.95	---	0.345	-1.41	0.06	-2.00	0.04	---	---	---	---	-1.40	0.01	-2.00	0.00
Soluble fraction 2/11/22	1.95	---	0.345	-1.39	0.09	-2.01	0.04	---	---	---	---				
Soluble fraction 1/13/21	0.25	---	0.916	---	---	---	---	---	---	---	---	---	---	---	---
Soluble fraction 2/13/21	0.25	---	0.916	---	---	---	---	---	---	---	---				
Ppt. fraction 1/ 0/25	---	0.00	0.000	---	---	---	---	---	---	---	---	---	---	---	---
Ppt. fraction 2/0/25	---	0.00	0.000	---	---	---	---	---	---	---	---				
Ppt. fraction 1/3/24	---	0.39	0.131	---	---	---	---	---	---	---	---	---	---	---	---

Ppt. fraction 2/3/24	---	0.39	0.131	---	---	---	---	---	---	---	---				
Ppt. fraction 1/9/23	---	0.79	0.264	0.89	0.07	1.29	0.03	0.87	0.03	1.27	0.03	0.83	0.07	1.23	0.07
				0.84	0.07	1.24	0.03								
Ppt. fraction 2/9/23	---	0.79	0.264	0.74	0.08	1.15	0.04	---	---	---	---				
Ppt. fraction 1/11/22	---	1.03	0.345	0.71	0.09	1.07	0.05	0.69	0.04	1.05	0.03	0.68	0.03	1.05	0.02
				0.66	0.05	1.03	0.03								
Ppt. fraction 2/11/22	---	1.03	0.345	0.66	0.09	1.04	0.04	---	---	---	---				
Ppt. fraction 1/13/21	---	2.73	0.916	-0.12	0.09	-0.14	0.04	-0.12	0.01	-0.14	0.00	-0.07	0.08	-0.10	0.10
				-0.13	0.07	-0.14	0.04								
Ppt. fraction 2/13/21	---	2.73	0.916	0.04	0.17	0.06	0.06	-0.01	0.07	-0.06	0.16				
Uninoculated Control															
Soluble fraction 1/0/25	2.89	0.00	---	-0.30	0.05	-0.53	0.03	-0.33	0.05	-0.52	0.00	-0.38	0.06	-0.55	0.03
				-0.37	0.11	-0.52	0.04								
Soluble fraction 2/0/25	2.89	0.00	---	-0.41	0.08	-0.57	0.04	-0.42	0.01	-0.58	0.02				
				-0.43	0.05	-0.59	0.03								
Soluble fraction 1/3/24	3.00	0.00	---	-0.32	0.11	-0.55	0.05	---	---	---	---	-0.41	0.11	-0.62	0.08
Soluble fraction 2/3/24	3.00	0.00	---	-0.53	0.05	-0.71	0.02	-0.45	0.12	-0.65	0.08				
				-0.36	0.09	-0.60	0.04								
Soluble fraction	3.13	0.00	---	-0.54	0.06	-0.68	0.03	-0.58	0.05	-0.81	0.19	-0.50	0.09	-0.73	0.15
				-0.61	0.05	-0.94	0.04								

1/9/23															
Soluble fraction 2/9/23	3.13	0.00	---	-0.40	0.05	-0.65	0.02	-0.43	0.04	-0.64	0.02				
				-0.46	0.07	-0.63	0.04								
Soluble fraction 1/11/22	3.54	0.00	---	-0.29	0.07	-0.46	0.04	-0.25	0.05	-0.45	0.03	-0.31	0.08	-0.48	0.05
				-0.22	0.07	-0.43	0.04								
Soluble fraction 2/11/22	3.54	0.00	---	-0.36	0.06	-0.51	0.03	-0.38	0.02	-0.52	0.01				
				-0.39	0.09	-0.53	0.04								
Soluble fraction 1/13/21	3.83	0.00	---	-0.24	0.08	-0.44	0.03	---	---	---	---	-0.29	0.05	-0.44	0.02
Soluble fraction 2/13/21	3.83	0.00	---	-0.30	0.07	-0.47	0.03	-0.32	0.03	-0.45	0.03				
				-0.34	0.07	-0.43	0.03								

Table 4-3: Fe isotope compositions of the pure culture, F4, incubated at 40, 80 and 120 cm from the light and the uninoculated and dark controls. All cultures started at 25 ml total volume. Sampling volumes were always 1 ml, and were split into two 0.5 ml sub-volumes to obtain duplicate soluble and precipitate (ppt) fractions for that time point. Start volume is the volume of the culture on the day the sample was taken. Mmol Fe(III) is calculated by mass balance using the *Ferrozine* measurements for Fe(II). "*F*" represents the fraction of the total Fe(II)$_{aq}$ that has been oxidized. In the analyses column, up to triplicate mass spectrometry runs of a sample conducted on different days are reported; the errors are 2-SE from in-run statistics and reflect machine uncertainties and/or processing errors. The Mass Spec Average is the average of up to three analyses of a single sample, 1-SD is one standard deviation external; note that if there is only one mass spectrometry analysis, the error is 2-SE. The Average of Replicate is the average of processing replicates of a sample throughout the entire analytical procedure; the best estimate of external reproducibility. [1]per 0.5 ml split.

Table 4-3:

Sample/ Day/ Start Volume (ml)	Fe(II) mmol[1]	Fe(III) mmol[1]	F	Analyses				Mass Spec Average				Average of Replicates			
				$\delta^{56}Fe$	2-SE	$\delta^{57}Fe$	2-SE	$\delta^{56}Fe$	1-SD	$\delta^{57}Fe$	1-SD	$\delta^{56}Fe$	1-SD	$\delta^{57}Fe$	1-SD
F4 Culture - 40 cm															
Soluble fraction 1/0/25	4.66	---	0.000	-0.18	0.06	-0.28	0.03	---	---	---	---	-0.18	0.00	-0.22	0.08
Soluble fraction 2/0/25	4.66	---	0.000	-0.19	0.07	-0.17	0.04	---	---	---	---				
Soluble fraction 1/2/23	5.24	---	0.000	-0.13	0.07	-0.13	0.04	---	---	---	---	-0.13	0.01	-0.11	0.02
Soluble fraction 2/2/23	5.24	---	0.000	-0.14	0.06	-0.10	0.03	---	---	---	---				
Soluble fraction 1/4/21	4.58	---	0.017	-0.28	0.06	-0.48	0.03	-0.29	0.02	-0.41	0.11	-0.30	0.03	-0.39	0.08
				-0.30	0.05	-0.33	0.02								
Soluble fraction 2/4/21	4.58	---	0.017	-0.33	0.05	-0.35	0.03	---	---	---	---				
Soluble fraction 1/6/20	3.78	---	0.190	-0.77	0.06	-1.13	0.03	---	---	---	---	-0.78	0.03	-1.13	0.00
Soluble fraction 2/6/20	3.78	---	0.190	-0.80	0.05	-1.12	0.03	---	---	---	---				
Soluble fraction 1/8/19	2.01	---	0.570	-1.19	0.10	-1.76	0.05	-1.24	0.05	-1.85	0.08	-1.28	0.06	-1.85	0.06
				-1.28	0.05	-1.91	0.04								
				-1.26	0.04	-1.89	0.03								
Soluble	2.01	---	0.570	-1.34	0.05	-1.85	0.03	-1.34	0.01	-1.86	0.01				

fraction 2/8/19				-1.33	0.07	-1.87	0.03								
Soluble fraction 1/10/18	0.06	---	0.986	-2.44	0.10	-3.47	0.05	---	---	---	---	-2.39	0.06	-3.46	0.02
Soluble fraction 2/10/18	0.06	---	0.986	-2.35	0.07	-3.45	0.04	---	---	---	---				
Soluble fraction 1/12/17	0.00	---	1.00	---	---	---	---	---	---	---	---	---	---	---	---
Soluble fraction 2/12/17	0.00	---	1.00	---	---	---	---	---	---	---	---				
Soluble fraction 1/14/16	0.00	---	1.00	---	---	---	---	---	---	---	---	---	---	---	---
Soluble fraction 2/14/16	0.00	---	1.00	---	---	---	---	---	---	---	---				
Soluble fraction 1/16/15	0.00	---	1.00	---	---	---	---	---	---	---	---	---	---	---	---
Soluble fraction 2/16/15	0.00	---	1.00	---	---	---	---	---	---	---	---				
Ppt fraction 1/0/25	---	0.00	0.000	---	---	---	---	---	---	---	---	---	---	---	---
Ppt fraction 2/0/25	---	0.00	0.000	---	---	---	---	---	---	---	---				
Ppt fraction 1/2/23	---	0.00	0.000	---	---	---	---	---	---	---	---	---	---	---	---
Ppt	---	0.00	0.000	---	---	---	---	---	---	---	---				

fraction 2/2/23															
Ppt fraction 1/4/21	---	0.08	0.017	1.16	0.06	1.58	0.04	---	---	---	---	---	---	---	---
Ppt fraction 2/4/21	---	0.08	0.017	---	---	---	---	---	---	---	---				
Ppt fraction 1/6/20	---	0.88	0.190	0.72	0.04	1.01	0.02	---	---	---	---	0.64	0.09	1.00	0.09
Ppt fraction 2/6/20	---	0.88	0.190	0.66	0.05	1.09	0.03	0.60	0.08	1.00	0.13				
				0.54	0.05	0.91	0.03								
Ppt fraction 1/8/19	---	2.65	0.570	0.32	0.08	0.61	0.05	---	---	---	---	0.36	0.06	0.63	0.04
Ppt fraction 2/8/19	---	2.65	0.570	0.40	0.06	0.66	0.04	---	---	---	---				
Ppt fraction 1/10/18	---	4.60	0.986	-0.11	0.07	-0.09	0.04	-0.05	0.09	-0.08	0.02	0.00	0.09	0.01	0.10
				0.01	0.06	-0.06	0.03								
Ppt fraction 2/10/18	---	4.60	0.986	0.09	0.08	0.12	0.04	0.06	0.05	0.09	0.05				
				0.02	0.05	0.05	0.03								
Ppt fraction 1/12/17	---	4.66	1.00	---	---	---	---	---	---	---	---	---	---	---	---
Ppt fraction 2/12/17	---	4.66	1.00	---	---	---	---	---	---	---	---				
Ppt fraction 1/14/16	---	4.66	1.00	-0.11	0.06	-0.15	0.03	---	---	---	---	-0.08	0.04	-0.11	0.07
Ppt	---	4.66	1.00	-0.05	0.06	-0.06	0.04	---	---	---	---				

fraction 2/14/16															
Ppt fraction 1/16/15	---	4.66	1.00	---	---	---	---	---	---	---	---	---	---	---	---
Ppt fraction 2/16/15	---	4.66	1.00	-0.08	0.04	-0.03	0.03	---	---	---	---				
F4 Culture - 80 cm															
Soluble fraction 1/0/25	4.74	---	0.000	-0.20	0.05	-0.24	0.02	---	---	---	---	-0.18	0.03	-0.28	0.07
Soluble fraction 2/0/25	4.74	---	0.000	-0.16	0.08	-0.33	0.04	---	---	---	---				
Soluble fraction 1/2/24	5.16	---	0.000	---	---	---	---	---	---	---	---	---	---	---	---
Soluble fraction 2/2/24	5.16	---	0.000	-0.18	0.05	-0.28	0.03	---	---	---	---				
Soluble fraction 1/4/23	4.87	---	0.000	---	---	---	---	---	---	---	---	---	---	---	---
Soluble fraction 2/4/23	4.87	---	0.000	-0.22	0.05	-0.24	0.03	---	---	---	---				
Soluble fraction 1/6/22	5.25	---	0.000	---	---	---	---	---	---	---	---	---	---	---	---
Soluble fraction 2/6/22	5.25	---	0.000	-0.56	0.07	-0.87	0.03	-0.54	0.02	-0.83	0.06				
				-0.53	0.05	-0.80	0.03								
Soluble fraction 1/8/21	4.67	---	0.016	---	---	---	---	---	---	---	---	---	---	---	---

Soluble fraction 2/8/21	4.67	---	0.016	-0.44	0.07	-0.64	0.04	-0.46	0.04	-0.63	0.01				
				-0.51	0.05	-0.63	0.02								
				-0.43	0.03	-0.62	0.03								
Soluble fraction 1/10/20	4.42	---	0.067	-0.76	0.05	-1.04	0.03	---	---	---	---	-0.78	0.06	-1.15	0.10
Soluble fraction 2/10/20	4.42	---	0.067	-0.73	0.08	-1.19	0.04	-0.79	0.09	-1.20	0.02				
				-0.85	0.06	-1.22	0.03								
Soluble fraction 1/12/19	4.02	---	0.152	---	---	---	---	---	---	---	---	---	---	---	---
Soluble fraction 2/12/19	4.02	---	0.152	---	---	---	---	---	---	---	---				
Soluble fraction 1/14/18	3.80	---	0.198	---	---	---	---	---	---	---	---	---	---	---	---
Soluble fraction 2/14/18	3.80	---	0.198	-1.27	0.08	-1.85	0.04	-1.27	0.00	-1.85	0.00				
				-1.27	0.06	-1.85	0.04								
Soluble fraction 1/16/17	3.13	---	0.339	---	---	---	---	---	---	---	---	---	---	---	---
Soluble fraction 2/16/17	3.13	---	0.339	---	---	---	---	---	---	---	---				
Soluble fraction 1/18/16	2.68	---	0.434	-1.31	0.04	-1.90	0.03	---	---	---	---	-1.35	0.05	-1.94	0.06
Soluble fraction 2/18/16	2.68	---	0.434	-1.39	0.05	-1.98	0.02	---	---	---	---				
Soluble fraction 1/20/15	1.80	---	0.621	-2.48	0.04	-3.63	0.03	---	---	---	---	---	---	---	---

87

Soluble fraction 2/20/15	1.80	---	0.621	---	---	---	---	---	---	---	---				
Ppt fraction 1/0/25	---	0.00	0.000	---	---	---	---	---	---	---	---	---	---	---	---
Ppt fraction 2/0/25	---	0.00	0.000	---	---	---	---	---	---	---	---				
Ppt fraction 1/2/24	---	0.00	0.000	---	---	---	---	---	---	---	---	---	---	---	---
Ppt fraction 2/2/24	---	0.00	0.000	---	---	---	---	---	---	---	---				
Ppt fraction 1/4/23	---	0.00	0.000	---	---	---	---	---	---	---	---	---	---	---	---
Ppt fraction 2/4/23	---	0.00	0.000	---	---	---	---	---	---	---	---				
Ppt fraction 1/6/22	---	0.00	0.000	1.14	0.06	1.71	0.02	---	---	---	---	1.05	0.12	1.62	0.14
Ppt fraction 2/6/22	---	0.00	0.000	0.97	0.07	1.52	0.04	---	---	---	---				
Ppt fraction 1/8/21	---	0.08	0.016	---	---	---	---	---	---	---	---	---	---	---	---
Ppt fraction 2/8/21	---	0.08	0.016	0.93	0.06	1.38	0.04	0.90	0.03	1.36	0.02				
				0.88	0.04	1.34	0.02								
Ppt fraction 1/10/20	---	0.32	0.067	0.44	0.06	0.73	0.03	0.51	0.09	0.75	0.03	0.52	0.07	0.74	0.04
				0.57	0.04	0.77	0.03								

Ppt fraction 2/10/20	---	0.32	0.067	0.48	0.09	0.68	0.05	0.53	0.07	0.72	0.07				
				0.58	0.05	0.77	0.03								
Ppt fraction 1/12/19	---	0.72	0.152	---	---	---	---	---	---	---	---	---	---	---	---
Ppt fraction 2/12/19	---	0.72	0.152	---	---	---	---	---	---	---	---				
F4 Culture - 80 cm cont.															
Ppt fraction 1/14/18	---	0.94	0.198	0.32	0.05	0.46	0.03	---	---	---	---	0.31	0.02	0.40	0.05
Ppt fraction 2/14/18	---	0.94	0.198	0.33	0.06	0.38	0.04	0.31	0.03	0.37	0.02				
				0.29	0.07	0.35	0.03								
Ppt fraction 1/16/17	---	1.61	0.339	---	---	---	---	---	---	---	---	---	---	---	---
Ppt fraction 2/16/17	---	1.61	0.339	---	---	---	---	---	---	---	---				
Ppt fraction 1/18/16	---	2.06	0.434	0.44	0.04	0.63	0.02	---	---	---	---	0.36	0.12	0.60	0.05
Ppt fraction 2/18/16	---	2.06	0.434	0.28	0.05	0.56	0.03	---	---	---	---				
Ppt fraction 1/20/15	---	2.95	0.621	0.24	0.06	0.43	0.04	---	---	---	---	---	---	---	---
Ppt fraction 2/20/15	---	2.95	0.621	---	---	---	---	---	---	---	---				

F4 Culture - 120 cm														
Soluble fraction 1/0/25	4.90	---	0.000	-0.22	0.06	-0.28	0.04	---	---	---	---	---	---	---	---
Soluble fraction 2/0/25	4.90	---	0.000	---	---	---	---	---	---	---	---				
Soluble fraction 1/2/24	5.23	---	0.000	-0.19	0.03	-0.17	0.03	---	---	---	---	-0.15	0.05	-0.19	0.02
Soluble fraction 2/2/24	5.23	---	0.000	-0.12	0.05	-0.21	0.03	---	---	---	---				
Soluble fraction 1/4/23	4.97	---	0.000	-0.22	0.05	-0.30	0.03	---	---	---	---	-0.21	0.02	-0.31	0.00
Soluble fraction 2/4/23	4.97	---	0.000	-0.19	0.06	-0.31	0.03	---	---	---	---				
Soluble fraction 1/6/22	5.47	---	0.000	-0.41	0.04	-0.58	0.03	---	---	---	---	---	---	---	---
Soluble fraction 2/6/22	5.47	---	0.000	---	---	---	---	---	---	---	---				
Soluble fraction 1/8/21	5.29	---	0.000	-0.32	0.06	-0.45	0.03	---	---	---	---	-0.28	0.05	-0.44	0.01
Soluble fraction 2/8/21	5.29	---	0.000	-0.25	0.05	-0.43	0.04	---	---	---	---				
Soluble fraction 1/10/20	5.42	---	0.000	-0.48	0.07	-0.73	0.04	---	---	---	---	---	---	---	---
Soluble fraction	5.42	---	0.000	---	---	---	---	---	---	---	---				

2/10/20															
Soluble fraction 1/12/19	5.27	---	0.000	-0.43	0.07	-0.63	0.03	---	---	---	---	-0.43	0.01	-0.67	0.04
Soluble fraction 2/12/19	5.27	---	0.000	-0.44	0.03	-0.70	0.03	---	---	---	---				
Soluble fraction 1/14/18	5.38	---	0.000	-0.74	0.04	-1.10	0.03	---	---	---	---	---	---	---	---
Soluble fraction 2/14/18	5.38	---	0.000	---	---	---	---	---	---	---	---				
Soluble fraction 1/16/17	4.91	---	0.000	-0.70	0.08	-0.98	0.04	---	---	---	---	---	---	---	---
Soluble fraction 2/16/17	4.91	---	0.000	---	---	---	---	---	---	---	---				
Soluble fraction 1/18/16	4.80	---	0.020	-0.70	0.03	-1.01	0.03	---	---	---	---	---	---	---	---
Soluble fraction 2/18/16	4.80	---	0.020	---	---	---	---	---	---	---	---				
Soluble fraction 1/20/15	4.24	---	0.134	---	---	---	---	---	---	---	---	---	---	---	---
Soluble fraction 2/20/15	4.24	---	0.134	-0.66	0.05	-0.94	0.04	-0.68	0.03	-0.99	0.07				
				-0.70	0.04	-1.04	0.02								
Ppt fraction 1/0/25	---	0.00	0.000	---	---	---	---	---	---	---	---	---	---	---	---
Ppt fraction	---	0.00	0.000	---	---	---	---	---	---	---	---				

2/0/25															
Ppt fraction 1/2/24	---	0.00	0.000	---	---	---	---	---	---	---	---	---	---	---	---
Ppt fraction 2/2/24	---	0.00	0.000	---	---	---	---	---	---	---	---				
Ppt fraction 1/4/23	---	0.00	0.000	---	---	---	---	---	---	---	---	---	---	---	---
Ppt fraction 2/4/23	---	0.00	0.000	---	---	---	---	---	---	---	---				
Ppt fraction 1/6/22	---	0.00	0.000	0.98	0.06	1.45	0.03	---	---	---	---	---	---	---	---
Ppt fraction 2/6/22	---	0.00	0.000	---	---	---	---	---	---	---	---				
Ppt fraction 1/8/21	---	0.00	0.000	1.48	0.06	2.27	0.04	---	---	---	---	---	---	---	---
Ppt fraction 2/8/21	---	0.00	0.000	---	---	---	---	---	---	---	---				
Ppt fraction 1/10/20	---	0.00	0.000	---	---	---	---	---	---	---	---	---	---	---	---
Ppt fraction 2/10/20	---	0.00	0.000	---	---	---	---	---	---	---	---				
Ppt fraction 1/12/19	---	0.00	0.000	0.94	0.06	1.48	0.03	---	---	---	---	---	---	---	---
Ppt fraction	---	0.00	0.000	---	---	---	---	---	---	---	---				

2/12/19															
Ppt fraction 1/14/18	---	0.00	0.000	0.55	0.07	0.86	0.03	0.59	0.06	0.87	0.02	---	---	---	---
				0.63	0.05	0.88	0.02								
Ppt fraction 2/14/18	---	0.00	0.000	---	---	---	---	---	---	---	---				
Ppt fraction 1/16/17	---	0.00	0.000	0.76	0.09	1.12	0.04	---	---	---	---	---	---	---	---
Ppt fraction 2/16/17	---	0.00	0.000	---	---	---	---	---	---	---	---				
Ppt fraction 1/18/16	---	0.10	0.020	0.68	0.05	1.08	0.03	---	---	---	---	---	---	---	---
Ppt fraction 2/18/16	---	0.10	0.020	---	---	---	---	---	---	---	---				
Ppt fraction 1/20/15	---	0.65	0.134	0.35	0.05	0.52	0.02	---	---	---	---	0.27	0.08	0.44	0.11
Ppt fraction 2/20/15	---	0.65	0.134	0.30	0.06	0.42	0.03	0.24	0.06	0.42	0.11				
				0.25	0.05	0.53	0.02								
				0.17	0.06	0.30	0.03								
Uninoculated Control															
Soluble fraction 1/0/25	4.98	0.00	---	-0.18	0.06	-0.27	0.04	---	---	---	---	-0.16	0.03	-0.20	0.09
Soluble fraction 2/0/25	4.98	0.00	---	-0.14	0.07	-0.14	0.04	---	---	---	---				
Soluble fraction 1/2/24	5.45	0.00	---	-0.24	0.06	-0.30	0.03	-0.20	0.06	-0.23	0.09	-0.20	0.04	-0.24	0.07
				-0.16	0.09	-0.17	0.04								
Soluble	5.45	0.00	---	-0.21	0.05	-0.24	0.04	---	---	---	---				

fraction 2/2/24															
Soluble fraction 1/4/23	5.33	0.00	---	-0.19	0.05	-0.26	0.02	---	---	---	---	-0.15	0.06	-0.22	0.06
Soluble fraction 2/4/23	5.33	0.00	---	-0.11	0.06	-0.18	0.03	---	---	---	---				
Soluble fraction 1/6/22	5.79	0.00	---	-0.26	0.08	-0.34	0.04	---	---	---	---	-0.26	0.01	-0.32	0.02
Soluble fraction 2/6/22	5.79	0.00	---	-0.27	0.05	-0.31	0.03	---	---	---	---				
Soluble fraction 1/8/21	5.83	0.00	---	-0.16	0.04	-0.21	0.03	---	---	---	---	-0.13	0.04	-0.21	0.01
Soluble fraction 2/8/21	5.83	0.00	---	-0.09	0.04	-0.20	0.02	---	---	---	---				
Soluble fraction 1/10/20	6.20	0.00	---	-0.24	0.08	-0.35	0.04	---	---	---	---	-0.19	0.07	-0.29	0.08
Soluble fraction 2/10/20	6.20	0.00	---	-0.14	0.07	-0.24	0.04	---	---	---	---				
Soluble fraction 1/12/19	6.31	0.00	---	-0.11	0.07	-0.14	0.04	---	---	---	---	-0.14	0.04	-0.20	0.08
Soluble fraction 2/12/19	6.31	0.00	---	-0.17	0.07	-0.26	0.03	---	---	---	---				
Soluble fraction 1/14/18	7.00	0.00	---	-0.26	0.07	-0.31	0.03	-0.18	0.09	-0.22	0.11	-0.21	0.09	-0.24	0.11
				-0.08	0.06	-0.09	0.03								
				-0.21	0.05	-0.25	0.03								
Soluble	7.00	0.00	---	-0.27	0.04	-0.32	0.03	---	---	---	---				

fraction 2/14/18															
Soluble fraction 1/16/17	6.92	0.00	---	-0.16	0.05	-0.14	0.03	---	---	---	---	-0.11	0.06	-0.16	0.03
Soluble fraction 2/16/17	6.92	0.00	---	-0.07	0.05	-0.18	0.03	---	---	---	---				
Soluble fraction 1/18/16	7.77	0.00	---	-0.18	0.05	-0.25	0.03	---	---	---	---	-0.14	0.06	-0.23	0.03
Soluble fraction 2/18/16	7.77	0.00	---	-0.10	0.05	-0.21	0.03	---	---	---	---				
Soluble fraction 1/20/15	7.88	0.00	---	-0.11	0.06	-0.21	0.04	---	---	---	---	-0.16	0.07	-0.22	0.01
Soluble fraction 2/20/15	7.88	0.00	---	-0.21	0.05	-0.22	0.03	---	---	---	---				
Dark Control															
Soluble fraction 1/0/25	5.01	0.00	---	---	---	---	---	---	---	---	---	---	---	---	---
Soluble fraction 2/0/25	5.01	0.00	---	---	---	---	---	---	---	---	---				
Soluble fraction 1/2/25	5.42	0.00	---	-0.21	0.09	-0.31	0.04	---	---	---	---	-0.18	0.04	-0.28	0.04
Dark control cont.															
Soluble fraction 2/2/25	5.42	0.00	---	-0.15	0.05	-0.25	0.03	---	---	---	---				

95

Soluble fraction 1/4/24	5.25	0.00	---	-0.17	0.06	-0.24	0.04	---	---	---	---	-0.20	0.05	-0.27	0.04
Soluble fraction 2/4/24	5.25	0.00	---	-0.24	0.04	-0.29	0.03	---	---	---	---				
Soluble fraction 1/6/23	5.75	0.00	---	-0.22	0.05	-0.29	0.03	---	---	---	---	-0.24	0.03	-0.32	0.04
Soluble fraction 2/6/23	5.75	0.00	---	-0.26	0.04	-0.35	0.03	---	---	---	---				
Soluble fraction 1/8/22	5.83	0.00	---	-0.15	0.08	-0.30	0.04	---	---	---	---	-.18	0.04	-0.28	0.04
Soluble fraction 2/8/22	5.83	0.00	---	-0.21	0.04	-0.25	0.02	---	---	---	---				
Soluble fraction 1/10/21	6.10	0.00	---	-0.18	0.05	-0.26	0.03	---	---	---	---	---	---	---	---
Soluble fraction 2/10/21	6.10	0.00	---	---	---	---	---	---	---	---	---				
Soluble fraction 1/12/20	6.40	0.00	---	-0.11	0.05	-0.17	0.04	---	---	---	---	-0.12	0.01	-0.17	0.00
Soluble fraction 2/12/20	6.40	0.00	---	-0.13	0.05	-0.17	0.03	---	---	---	---				
Soluble fraction 1/14/19	6.89	0.00	---	-0.19	0.05	-0.33	0.03	---	---	---	---	-0.20	0.02	-0.30	0.04
Soluble fraction 2/14/19	6.89	0.00	---	-0.22	0.05	-0.27	0.03	---	---	---	---				

Soluble fraction 1/16/18	7.10	0.00	---	-0.18	0.07	-0.17	0.04	---	---	---	---	-0.17	0.02	-0.16	0.01
Soluble fraction 2/16/18	7.10	0.00	---	-0.16	0.04	-0.15	0.03	---	---	---	---				
Soluble fraction 1/18/17	7.73	0.00	---	-0.27	0.07	-0.31	0.04	---	---	---	---	-0.20	0.09	-0.27	0.05
Soluble fraction 2/18/17	7.73	0.00	---	-0.14	0.06	-0.24	0.03	---	---	---	---				
Soluble fraction 1/20/16	8.28	0.00	---	-0.16	0.06	-0.28	0.03	---	---	---	---	-0.19	0.03	-0.26	0.12
Soluble fraction 2/20/16	8.28	0.00	---	-0.22	0.05	-0.37	0.03	-0.20	0.03	-0.26	0.17				
				-0.18	0.05	-0.14	0.04								

Molecular techniques

Denaturing gradient gel electrophoresis (DGGE)

To define and compare the phylogenetic diversity within the enrichment cultures to strain F4, genomic DNA was extracted from cultures of the two enrichments and strain F4 grown photoautotrophically on Fe(II) according to the protocol of Wilson (1995). In addition, approximately 5 mg of sodium hydrosulfite was added to the DNA extraction to reduce and solubilize Fe(III) precipitates in the culture. The extracted genomic DNA was used as a template for 16S rDNA amplification by standard PCR methods on a MasterCycler Gradient PCR machine (Eppendorf) using the primers GM5-GC (5' to 3': CGCCCGCCGCGCCCCGCGCCCGTCCCGCCGCCCCCGCCCGCCTACGGGA GGCAGCAG and 907M (5' to 3': CCGTCAATTCMTTTGAGTTT). The PCR program was as follows: 95°C for 1 min and then 24 cycles of 95°C for 1 min., 50°C for 1 min., and 72°C for 1.5 min, after which there was a 10 min extension time at 72°C. Amplification was confirmed by agarose gel electrophoresis (1% agarose). Following the protocols of Muyzer et al. (1998a), the amplified PCR products were separated on a 1.5 mm thick, polyacrylamide (6% (w/v)) gel containing a gradient of 20-60% urea and formamide as denaturants (where 100% denaturant contained 7 M urea and 40% v/v formamide). The gradient gel was made using a Bio-Rad model 385 gradient former and a Bio Rad EconoPump model EPI (10 ml/min) (Hercules, CA) and DGGE was conducted with a Bio-Rad D-gene system in TAE buffer at 200 Volts for 4 hours at 60°C.

Restriction fragment length polymorphism (RFLP)

For community analysis by RFLP, genomic DNA from the three cultures grown photoautotrophically on Fe(II) was extracted with the DNeasyTM Tissue Kit (Qiagen, Valencia, CA). Again, the extracted DNA was used as a template for 16S rDNA amplification as described above, in this case, using the primers 8F (5' to 3': AGAGTTTGATCCTGGCTCAG) and 1492R (5' to 3': GGTTACCTTGTTACGACTT). The PCR program here was: 94°C for 3 min and then 30 cycles of 94°C for 1 min., 55°C for 1 min., and 72°C for 1 min, after which there was a 10 min extension time at 72°C. After confirmation of amplification by agarose gel electrophoresis, the PCR products were cloned using the TOPO TA Cloning kit (Invitrogen, Carlsbad, CA) and transformed into E. coli. Plasmids were purified from approximately 95 clone-containing E. coli colonies for each of the three cultures by a high-throughput alkaline lysis procedure [127], and the purified plasmid product was used as a template to re-amplify the 16S rDNA insert using primers T3 (5' to 3': TAATACGACTCACTATA), and T7 (5' to 3': ATTAACCCTCACTAAAGGGA). The subsequent PCR products were digested with the enzymes HinP1 I and Msp I (New England Biolabs, final concentrations of 20 and 40 units of enzyme/ml respectively) overnight at 37°C and separated by electrophoresis on a 2.5% low melting point agarose gel. The clones were visually grouped into unique restriction pattern groups and representative clones from the largest groups were partially sequenced using the primer T3 and preliminarily identified using the Basic Local Alignment Search Tool (BLAST) [2]. For complete sequencing of the 16S rDNA gene clone of strain F4, the primers

T3, T7, and the bacterial primers 50F (5' to 3': AACACATGCAAGTCGAACG), 356F (5' to 3': ACTCCTACGGGAGGCAGCA), 515F (5' to 3': GTGCCAGCMGCCGCGGTAA), 805F (5' to 3': ATTAGATACCCTGGTAGTC), 926R (5' to 3': ACCGCTTGTGCGGGCCC) and 1200R (5' to 3': TCGTAAGGGCCATGATG) were used. Sequencing was performed at the DNA Sequencing Core Facility at the Beckman Institute at Caltech. The resultant sequences were edited and aligned using Sequencer (GeneCodes Corp.). Distance, parsimony and maximum likelihood phylogenetic trees were constructed using the ARB software package [165], and compared to determine the relative robustness of the resulting phylogenetic tree topologies.

Mineral analyses

Raman spectroscopy

For analysis of the biological precipitates by Raman spectroscopy, approximately one-week-old cultures of strain F4 and the two enrichments were transferred to an anaerobic chamber where 1 ml of culture containing rust-colored precipitates was taken with a syringe and transferred to a microcentrifuge tube. The precipitates were collected by centrifugation and incubated at room temperature for approximately 12 hours in 2.25% sodium hypochlorite (Chlorox) to remove residual organic materials. Controls where the precipitates were not subjected to sodium hypochlorite showed that this treatment only increased the signal to noise ratio and did not alter the Fe mineral phases (data not shown). The precipitates were washed three times with ultra-pure H_2O that had been

equilibrated with an anoxic atmosphere and the precipitates were immediately

analyzed on a Renishaw Micro Raman spectrometer operating with a 514.5 nm

argon laser at a power of 0.5 mW using a 5x, 20x, and/or 100x objective.

Multiple areas of the precipitates in all the cultures were analyzed to address the

homogeneity of the material. Phases of the precipitates were identified by

comparison to a standard database as well as to 2-line ferrihydrite and goethite

(α-FeOOH) prepared according to Schwertmann and Cornell (1991).

Powder X-Ray diffraction

For analysis of the biological precipitates by powder x-ray diffraction

(XRD), an approximately two and a half week-old culture of strain F4 was

transferred to an anoxic chamber where 1 ml was removed with a syringe. The

precipitates were collected by centrifugation and residual organic materials were

oxidized with sodium hypochlorite as described above. The precipitates were

washed three times with ultra-pure H2O that was equilibrated with an anoxic

atmosphere, spread on a glass disk, and allowed to dry in an anaerobic

chamber. XRD patters were obtained on a Scintag Pad V X-ray Powder

Diffractometer using Cu-Kα radiation operating at a 35 kV and 30 mA and a θ-2θ

goniometer equipped with a germanium solid-state detector. Each scan used a

0.04° step size starting at 10° and ending at 80° with a counting time of 2

seconds per step. Phases of the precipitates were identified by comparison to

spectra in the PCPDFWIN program, © JCPDS-International Centre for Diffraction

Data, 1997, as well as to spectra obtained from synthetic 2-line ferrihydrite and

α-FeOOH.

Standards and nomenclature

The two Fe isotope ratios measured in this study are reported as ^{56}Fe

/^{54}Fe and 57Fe/^{54}Fe ratios in standard δ notation in units of per mil (‰), where:

(1) δ^{56}Fe ‰ = [(^{56}Fe /^{54}Fe)$_{SAMPLE}$/(^{56}Fe /^{54}Fe)$_{WHOLE-EARTH}$)-1] 10^3

and

(2) δ^{57}Fe‰ = [(^{57}Fe/^{54}Fe) $_{SAMPLE}$ /(^{57}Fe/^{54}Fe) $_{WHOLE-EARTH}$)-1] 10^3

The ^{56}Fe /^{54}Fe whole-earth ratio is the average of 46 igneous rocks that have

δ^{56}Fe = 0.00±0.05‰. On this scale, the IRMM-14 Fe standard, available from the

Institute for Reference Materials and Measurements in Belgium, has a δ^{56}Fe

value of -0.09±0.05‰ and δ^{57}Fe value of -0.11±0.07‰ [11]. Co-variations in

δ^{56}Fe and δ^{57}Fe values plot along a linear array, whose slope is consistent with

mass-dependent fractionation, which provides an internal check for data integrity

[11]. Differences in isotope composition between two components A and B are

expressed in standard notation as:

3) $\Delta_{A-B} = \delta^{56}Fe_A - \delta^{56}Fe_B$

Experimental details

For the first set of Fe isotope fractionation experiments, single cultures of

the two enrichments and an uninoculated medium blank were incubated at a

distance of 40 cm from the incandescent light source. The isotopic compositions

of the starting reagents and culture inoculums for this experiment are listed in Table 4-1. All sampling was conducted under strictly anoxic conditions in an anaerobic chamber. At each sampling point throughout the growth period, the cultures were shaken vigorously to homogenize the contents. The total $Fe(II)_{aq}$ concentration was measured by the *Ferrozine* assay [159], to calculate "*F*", the fraction of $Fe(II)_{aq}$ oxidized, and 1 ml from each culture was removed for isotope analysis. This 1 ml sample was divided into two 0.5 ml fractions, each of which was transferred to a separate microcentrifuge tube, producing two duplicate samples for each time point; these duplicates provide an assessment of the accuracy of separation of solid and liquid phases. Because the medium preparation procedures described above appeared to eliminate the formation of Fe(II) precipitates during photosynthetic Fe(II)-oxidation, the Fe(III) precipitate was isolated from $Fe(II)_{aq}$ solely by centrifugation. The Fe(II)-containing supernatant was removed with a pipette and filtered through a 0.22 μm nylon filter; the Fe(III) precipitate was washed twice with ultra-pure H_2O. The small changes to the total culture volume that occurred from successive sampling were accounted for in the calculation of *F*. All samples were stored at -80°C until chemical processing for isotope analysis could be performed.

In the second set of experiments, Fe isotope fractionation produced by strain F4 was measured. The experimental setup in this case was similar to that for the enrichments but with two differences. First, the overall rate of Fe(II)-oxidation was varied by incubating duplicate cultures of strain F4 inoculated with approximately the same number of cells at 40, 80 and 120 cm distances from the

light source, and second, duplicate cultures were incubated in the dark as a

control, in addition to duplicate uninoculated controls that were incubated in the

light. Preparation followed the same methods as those used for the enrichment

cultures.

Methods for isotopic analysis

Samples were quantitatively dissolved in 7 M HCl and chemically

separated from other cations and organic material by a previously described

column separation procedure [155, 164]. Briefly, the samples were subjected to

two passages through an anion exchange resin (Bio-Rad AG 1X4 200-400 mesh)

with 7.0 M double-distilled HCl as the eluent for matrix removal, and 0.5 M HCl

as the eluent for Fe collection. Yields were quantitative to avoid possible mass

fractionation during separation. After elution of the sample from the anion

exchange column and HCl was removed by evaporation. Samples were then

diluted to 400 ppb Fe using 0.1% Optima grade HNO_3 for isotope analysis. High-

precision Fe isotope measurements were made using a Micromass IsoProbe

multiple-collector inductively-coupled-plasma mass spectrometer (MC-ICP-MS)

at the University of Wisconsin-Madison. Technical aspects of the MC-ICP-MS

methods have been published in detail elsewhere [11, 155]. Instrumental mass

bias corrections were made using a standard-sample-standard approach. The

data were compared to theoretical models such as Rayleigh fractionation or

closed-system equilibration (*e.g.*, equations 3.28 and 3.20b, respectively, in

Criss, 1999), using $\alpha=1.0015$.

RESULTS

Physiological and phylogenetic characterization of the cultures

Photoautotrophic oxidation of Fe(II)

All three cultures used in this study are able to grow photoautotrophically using $Fe(II)_{aq}$ as an electron donor. An increase in cell numbers (data not shown) accompanied by oxidation of $Fe(II)_{aq}$ to rust-colored Fe(III) precipitates occurs in all three cultures over a period of 7 to 10 days after inoculation into anoxic medium where Fe(II) is the sole source of electrons (Figure 4-1). The maximal rates of Fe(II)-oxidation in these cultures at a 40 cm distance from the light source are ~1.5 mM Fe(II)/day for strain F4 (between days 6 and 8), ~1.9 mM Fe(II)/day for enrichment 1 (between days 9 and 11) and ~1.5 mM Fe(II)/day for enrichment 2 (between days 11 and 13); the fraction of the total Fe(II)-oxidized in these cultures at the end of the experiment was 100%, 92%, and 93%, respectively. Neither an increase in cell numbers nor Fe(II)-oxidation is observed when these cultures are incubated in the dark. No cell growth occurs when Fe(II) (*i.e.*, the electron donor) is omitted and the cultures are incubated in the light. Moreover, no component of the medium is able to oxidize Fe(II) abiotically as shown by the lack of Fe(II)-oxidation in uninoculated controls (Figure 4-1). Together, these results indicate that the observed Fe(II)-oxidation is biologically-mediated by a light-dependent reaction that is correlated to an increase in biomass. Stoichiometric demonstrations of growth on Fe(II) have been reported previously [52, 69, 70, 163].
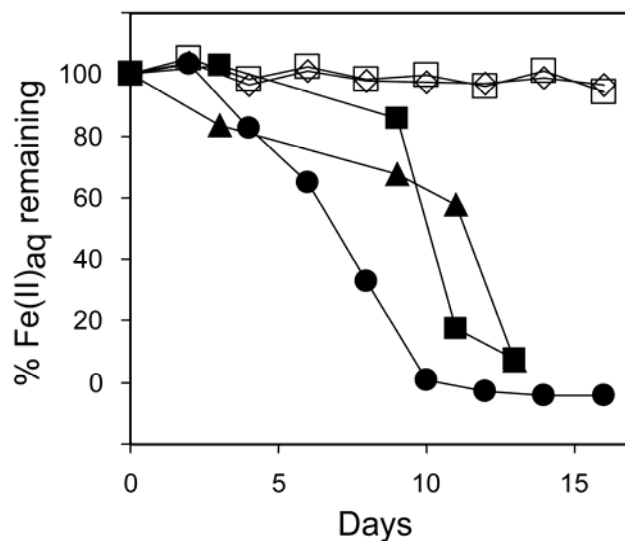
Figure 4-1: Fe(II)-oxidation by the two enrichment cultures and *Thiodictyon* strain F4. ● - F4, ■ - enrichment 1, ▲ - enrichment 2, □ - uninoculated control, ◇ - medium inoculated with F4, incubated in the dark. All cultures, except the dark control, were incubated at 40 cm from the 40 W light source. The dark control is representative of dark controls performed with the two enrichment cultures. Iron contents for the uninoculated and dark controls are consistent over time within analytical errors. Data for the enrichment cultures and *Thiodictyon* strain F4 were collected in separate experiments.

The effect of light intensity on the overall rate of biological Fe(II)-oxidation was investigated using duplicate cultures of strain F4 that were inoculated with approximately the same number of cells and incubated at various distances from the 40 W light source (40, 80, and 120 cm). As expected, the farther the cultures were from the light, the slower was their maximal rate of Fe(II)-oxidation (Figure 4-2). Maximal rates of ~1.5 mM Fe(II)/day, ~0.4 mM Fe(II)/day, and ~0.2 mM

Fe(II)/day were observed for the cultures at 40, 80, and 120 cm light distances, respectively. As a result, Fe(II) was oxidized to completion only in the strain F4 culture that was incubated at 40 cm from the light source within the timescale of the experiment (20 days).
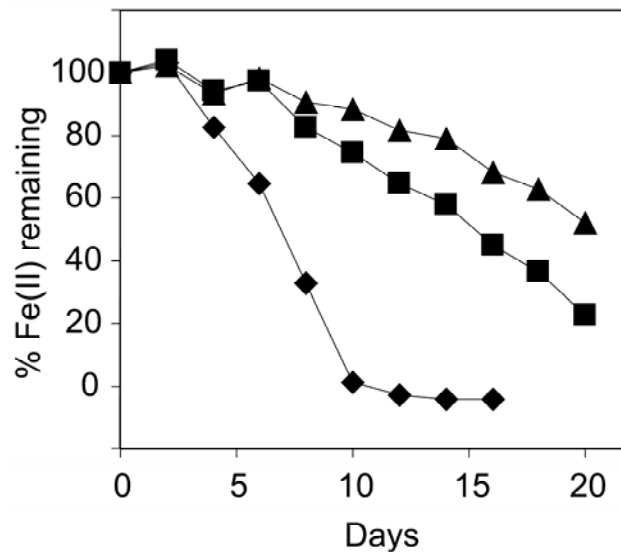
Figure 4-2: Fe(II)-oxidation by cultures of *Thiodictyon* strain F4 inoculated with approximately the same number of cells and incubated at 40, 80, and 120 cm from the light source. ◆ - F4 incubated at 40 cm from the light, ■ - 80 cm, ▲ - 120 cm. The data shown are representative of duplicate cultures.

Microscopy

Differential interference contrast (DIC) microscopy was used to visually characterize the three cultures. In the enrichment cultures, several morphotypes can be seen: all are rod-shaped, ranging in size from 0.5-1 μm wide and 1.5-2 μm long for the smallest cell type, to 1-1.5 μm wide and 4-5 μm long for the

largest, with some cells containing gas vacuoles (Figure 4-3A). Cells of strain F4

are approximately 1.5-2 µm wide and 5-7 µm long, contain gas vacuoles (Figure

4-3B), form long chains with side branches that give rise to net-like cell

arrangements, and have a purple-violet pigmentation when grown

photoheterotrophically on acetate. The variety of morphologies observed

indicates that multiple types of bacteria are represented among the three

cultures, although some cells in the enrichment cultures (*e.g.*, Type I, Figure 4-

3A) appear similar to strain F4.
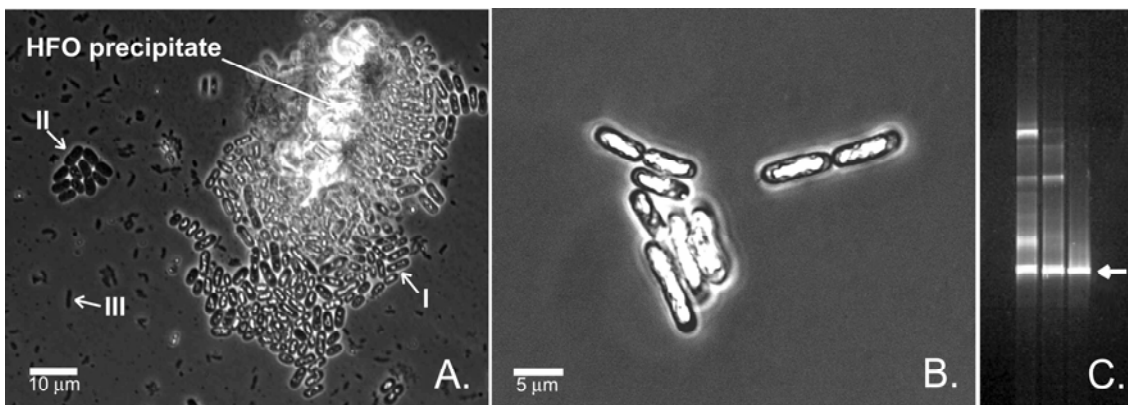
Figure 4-3: Differential interference contrast (DIC) micrographs of the

enrichments and *Thiodictyon* strain F4. A. A representative micrograph of the

two enrichments growing photosynthetically on 10 mM Fe(II)$_{aq}$ supplemented

with 1 mM acetate. Three major cell morphologies are observed: approximately

1-1.5 µm by 4-5 µm, rod shaped cells with gas vacuoles (light areas within the

cells) which tended to aggregate around the HFO precipitates (I), 1.5-2 µm by

3.5-4 µm rod shaped cells with no gas vesicles (II) and 0.5-1 µm by 1.5-2 µm rod

shaped cells (III). B. DIC micrograph of *Thiodictyon* strain F4, growing

photosynthetically on 10 mM Fe(II)$_{aq}$. Cells are approximately 1.5-2 µm by 5-7

µm and contain gas vacuoles. Note the similarity in size and shape between cells of *Thiodictyon* strain F4 and cells of type I in the enrichment culture. C. DGGE of the enrichments and *Thiodictyon* strain F4. From left to right lanes correspond to enrichment 1, enrichment 2 and *Thiodictyon* strain F4.

DGGE and RFLP analyses

To assess the diversity within our cultures, we used Denaturing Gradient Gel Electrophoresis (DGGE) and Restriction Fragment Length Polymorphism (RFLP) [30, 123]. DGGE and RFLP showed that multiple species are present in our enrichment cultures, corroborating the diversity of morphotypes observed by microscopy. An abundant organism in these cultures is very similar to strain F4 (DGGE results, Figure 4-3C; RFLP results not shown). Complete 16S rDNA sequence analysis of strain F4 showed that this isolate is a γ-Proteobacterium that groups with the *Thiorhodaceae* (Figure 4-4). The closest relative to this strain by 16S rDNA comparison (98% sequence identity, 1347 nucleotides considered) is the uncharacterized *Thiodictyon* strain Thd2 that is also able to oxidize Fe(II) phototrophically [52]. Other bacteria present in both of the enrichments were found to have sequences similar to the phototrophic Fe(II)-oxidizing strain *Chlorobium ferrooxidans* [69], and the Fe(III)-reducing heterotrophic genus *Geobacter* [110]. Preliminary RFLP data suggest that the abundance of Fe(III)-reducing organisms in the enrichments is low (data not shown), and thus it is unlikely that they appreciably affect the measured Fe isotope fractionations.
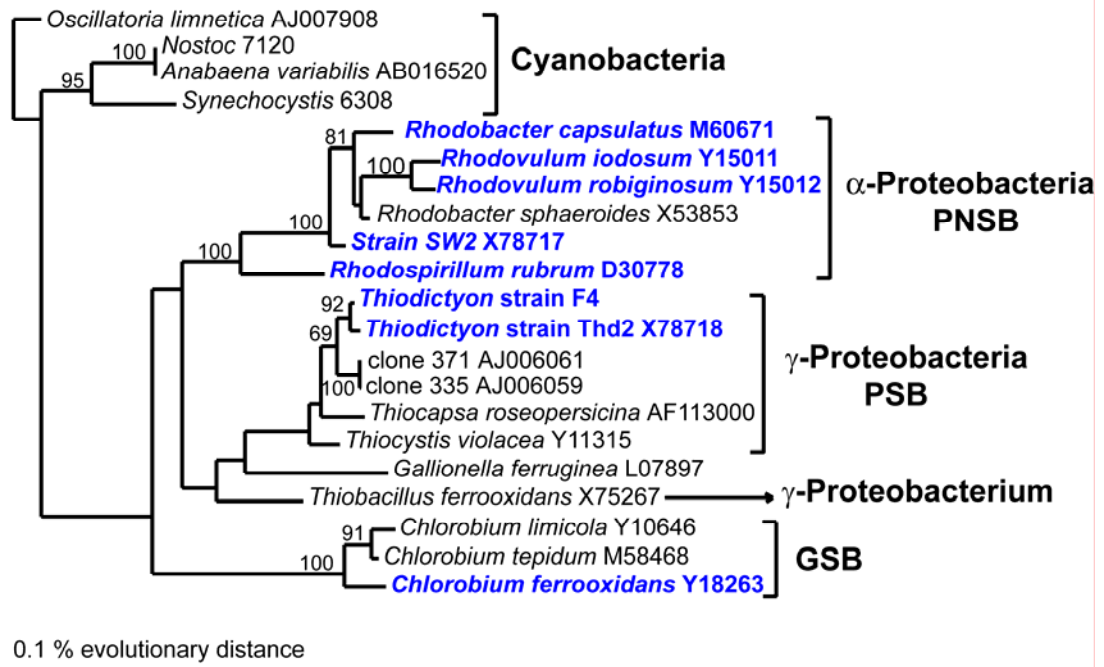
Figure 4-4: The phylogenetic relationship of *Thiodictyon* strain F4 inferred from

16S rDNA sequences. The tree was constructed by the maximum-likelihood

method using the ARB software package with 1250 positions considered.

Bootstrap values above 50% from 100 bootstrap analyses are given at branch

nodes. Anaerobic phototrophs able to oxidize Fe(II) are in blue to illustrate the

evolutionary diversity of organisms capable of this form of metabolism. Aerobic

phototrophs (cyanobacteria) and other organisms capable of oxidizing Fe(II) non-

photosynthetically are also shown for phylogenetic comparison. Accession

numbers are listed after the bacterium. PNSB – purple non sulfur bacteria, PSB

– purple sulfur bacteria, GSB – green sulfur bacteria.

Biological precipitates

The Raman spectra obtained using a 5x objective for the Fe(III) precipitates in all three cultures show either no distinctive peaks or generally resemble the spectrum obtained for synthetic 2-line ferrihydrite at the same laser power, with a broad peak ranging from approximately 950 to 1150 cm^{-1} (data not shown). The low signal to noise ratios in the spectra determined for the biological precipitates and the 2-line ferrihydrite synthetic reference, however, make it difficult to identify distinctive peaks. The peak at 950 to 1150 cm^{-1}, observed in our 2-line ferrihydrite standard, is not observed in the Raman spectrum of 2-line ferrihydrite published by Mazzetti and Thistlethwaite (2002). The spectrum of our 2-line ferrihydrite control analyzed under the 20x objective, however, more closely matches the published spectrum for this material with broad peaks at approximately 710, 1320, and 1550 cm^{-1}, and no broad peak at 950 to 1150 cm^{-1}. Subtle peaks at 290 and 400 cm^{-1} also exist in the spectrum we obtained for the 2-line ferrihydrite standard using the 20x objective. Under the 100x objective, these two peaks become more defined and intense and an additional intense peak at approximately 220 cm^{-1} is observed; these three peaks at approximately 200, 290 and 400 cm^{-1} are characteristic of hematite. A similar evolution of peaks was observed in the 2-line ferrihydrite spectrum of Mazzetti and Thistlethwaite (2002) after successive scans at increasing laser power. This suggests that thermal transformation of 2-line ferrihydrite to hematite occurred under the laser. As we increased the laser intensity on the biological precipitates, the spectra of the precipitates in all three cultures changed with

time, and eventually, spectra indicative of goethite were observed. This thermal transformation for both 2-line ferrihydrite and the biological precipitates occurs whether the same spot is analyzed at increasing laser intensity or new areas are chosen for analysis.

Because goethite is highly crystalline and our goethite standard produced a clear diagnostic spectrum at 5x objective power, if goethite had been present in significant amounts in our cultures, it would have been revealed using the 5x power objective. The fact that the ferric precipitates that formed in our cultures are easily transformed to goethite under the Raman laser suggests that they are unstable, and supports the interpretation that the primary precipitates are poorly crystalline hydrous ferric oxide (HFO); this is additionally supported by the 5x power Raman spectra on the solids, which gave little indication of diagnostic peaks. In no case were peaks in the Raman spectra found that correspond to vivianite or siderite.

Attempts to confirm the laser Raman spectroscopic results by XRD yielded inconclusive results due to the very fine-grained nature of the precipitates. Despite very slow scans (>18 hours), the two broad XRD peaks that are characteristic of 2-line ferrihydrite could not be discerned relative to background. Very small intensity peaks, only slightly higher than background, were observed for goethite and vivianite in the XRD spectra; no peaks matching those of siderite were observed (data not shown). As noted above, however, laser Raman spectra obtained at low power (where in situ conversion to goethite does not occur) did not reveal evidence for significant proportions of goethite,

vivianite, or siderite. We therefore conclude that poorly crystalline HFO

constituted the only significant solid material in the biologically-induced

precipitates.

Isotopic fractionation produced by the two enrichment cultures

Throughout the experiment with the enrichment cultures, the δ^{56}Fe values

for Fe(II)$_{aq}$ are always lower than those of the HFO precipitate in both enrichment

1 and 2 (Figure 4-5A and 5B). The isotopic fractionation between Fe(II)$_{aq}$ and

the HFO precipitate was relatively constant at early stages in reaction progress in

each of the cultures (Table 4-2). No Fe(II)-oxidation was observed in the

uninoculated control and no change in Fe isotope composition for Fe(II)$_{aq}$ over

time relative to the δ^{56}Fe value of the initial Fe(II) reagent in the medium was

observed (Figure 4-5C). This confirms that no significant precipitation of ferrous

solids or abiotic Fe(II)-oxidation (followed by precipitation of ferric (hydr)oxides)

occurred over the course of the experiment.
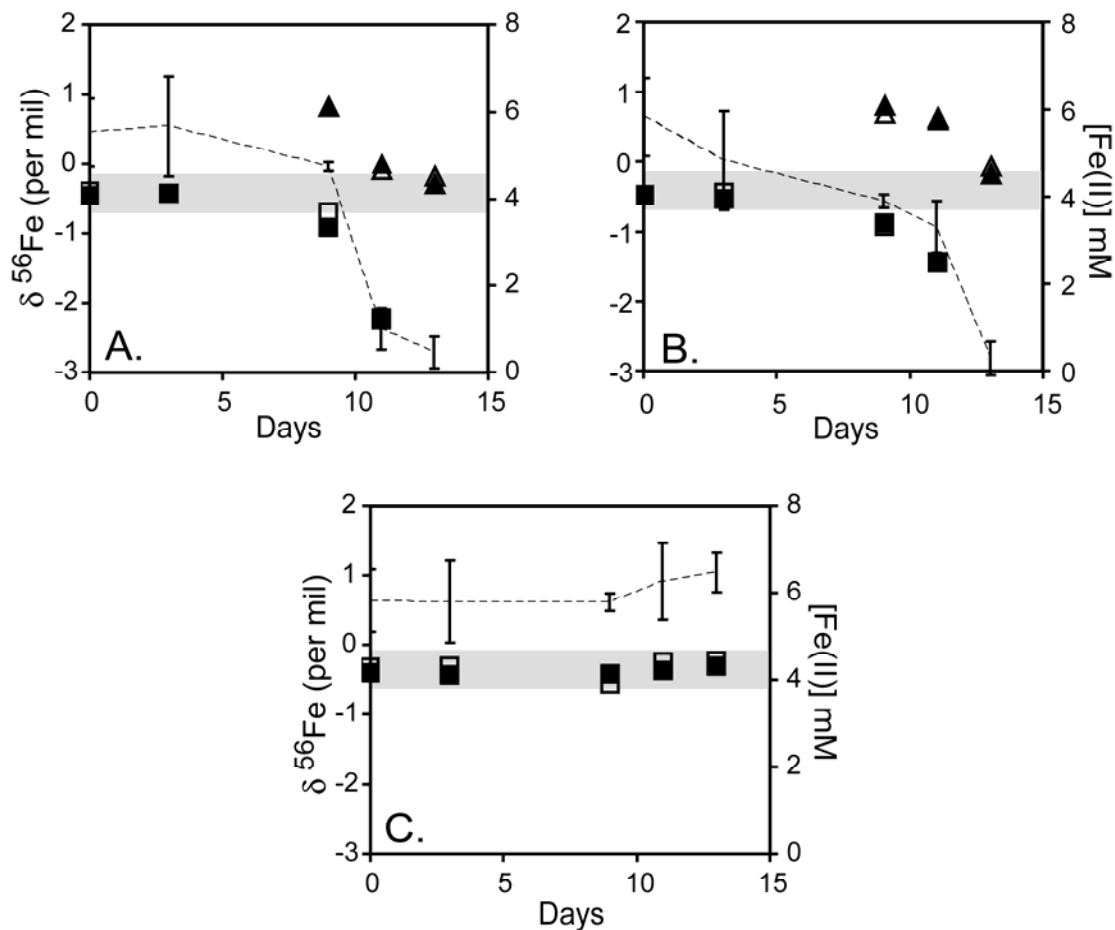
Figure 4-5: Isotopic data for the two enrichments incubated at 40 cm from the light source and the uninoculated control. The δ^{56}Fe values for duplicate samples of the Fe(II)$_{aq}$ and HFO fractions taken from single cultures are plotted as a function of time. A. Enrichment 1. ■ and □ - duplicate Fe(II)$_{aq}$ fractions. ▲ and △ - duplicate HFO fractions. B. Enrichment 2. ■ and □ - duplicate Fe(II)$_{aq}$ fractions. ▲ and △ - duplicate HFO fractions. C. The uninoculated control. ■ and □ - duplicate Fe(II)$_{aq}$ fractions. The dashed line plots on graphs A., B., and C. are Fe(II)$_{aq}$ concentrations (mM) as determined by *Ferrozine* assay and the error bars represent the error on triplicate assays for each time point. The shaded box on each of the graphs illustrates the error on the isotopic

measurements from the uninoculated control. In some cases the points are larger than the error.

Isotopic fractionation produced by Thiodictyon strain F4

Study of *Thiodictyon* strain F4 allowed us to circumvent the potential isotopic effects of multiple species in the enrichment cultures. In addition, using strain F4, we were able to assess potential kinetic or equilibrium isotope effects linked to the rate of overall Fe(II)-oxidation through variations in light intensity. As in the enrichment cultures, the data from the *Thiodictyon* strain F4 cultures show that Fe(II)$_{aq}$ had lower ^{56}Fe /^{54}Fe ratios as compared to the Fe(III) precipitate (Figure 4-6A, 6B and 6C). The isotopic fractionation between Fe(II)$_{aq}$ and the HFO precipitate remained relatively constant during the early stages of reaction progress (Table 4-3). The isotopic composition of the HFO precipitate at the end of the experiment was different for each incubation distance due to incomplete Fe(II)-oxidation in the 80 to 120 cm cultures vs. complete oxidation in the 40 cm cultures (Figure 4-6A, 6B, 6C and Table 4-3). The uninoculated and dark controls for *Thiodictyon* strain F4 showed no significant deviation in Fe isotope composition throughout the 20 days and the results from the two controls are identical within analytical error (Figure 4-6D, 6E and Table 4-3).
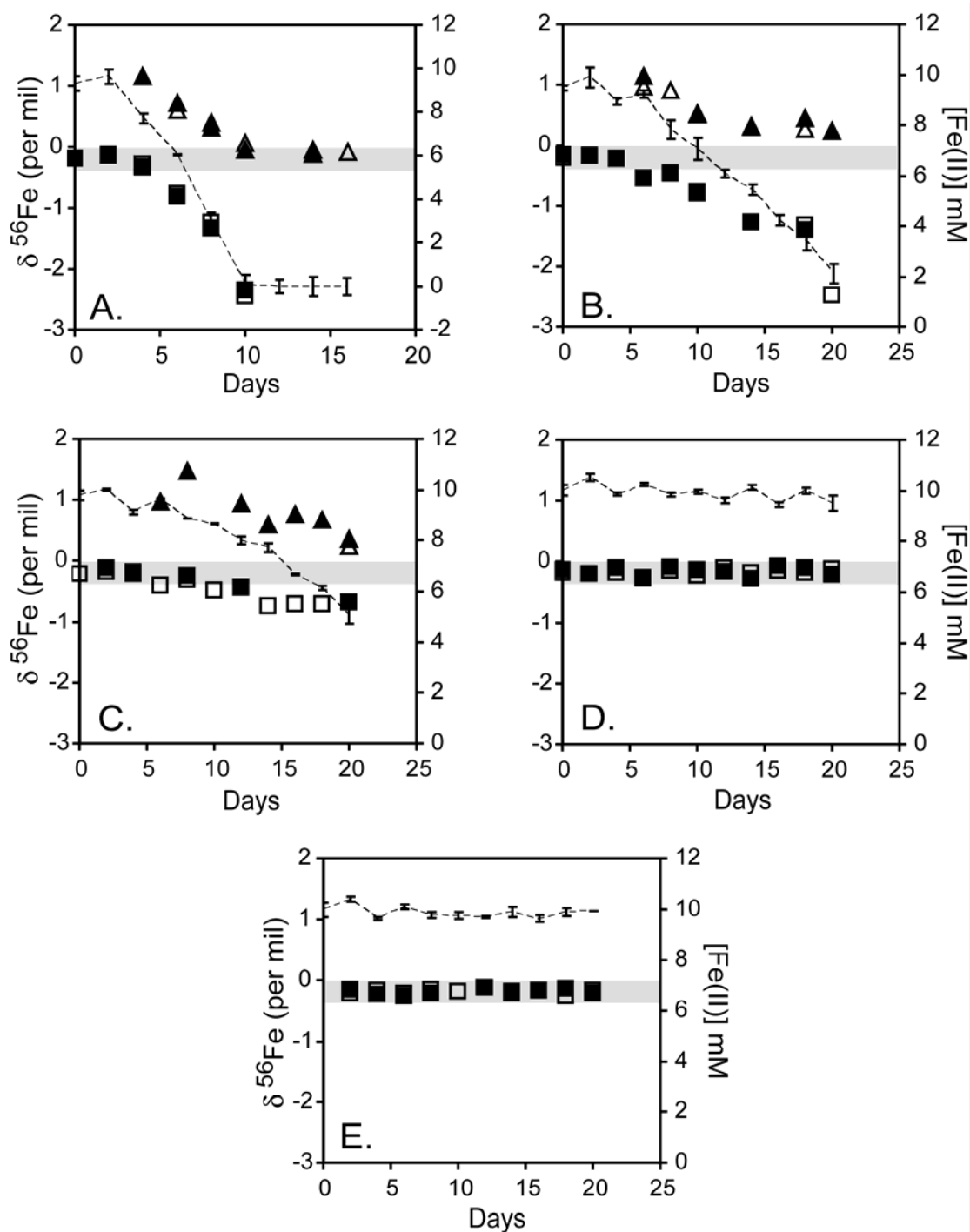
Figure 4-6: Isotopic data for *Thiodictyon* strain F4 incubated at 40, 80, and 120 cm from the light source and the uninoculated and dark controls. The δ^{56}Fe values for duplicate samples of the Fe(II)$_{aq}$ and HFO fractions taken from single cultures are plotted as a function of time. A. F4 incubated at 40 cm from the

light. ■ and □ - duplicate Fe(II)$_{aq}$ fractions. ▲ and △ - duplicate HFO fractions.

B. F4 incubated at 80 cm from the light. ■ and □ - duplicate Fe(II)$_{aq}$ fractions.

▲ and △ - duplicate HFO fractions. C. F4 incubated at 120 cm from the light.

■ and □ - duplicate Fe(II)$_{aq}$ fractions. ▲ and △ - duplicate HFO fractions. D

and E. The uninoculated and dark controls, respectively. ■ and □ - duplicate

Fe(II)$_{aq}$ fractions. The dashed line plots on graphs A., B., and C. are Fe(II)$_{aq}$

concentrations (mM) as determined by *Ferrozine* assay and the error bars

represent the error on triplicate assays for each time point. The shaded box on

each of the graphs illustrates the error on the isotopic measurements from the

uninoculated and dark controls. In some cases the plotted points are larger than

the error.

DISCUSSION

Isotopic fractionation mechanisms: general observations

The isotopic fractionation between Fe(II)$_{aq}$ and the HFO precipitate is

relatively constant (~ -1.5±0.2‰) for the enrichment and *Thiodictyon* strain F4

experiments during early stages in the reaction progress ("*F*") (Figure 4-7A, 7B,

and Table 4-4) and appear to be independent of the Fe(II)-oxidation rate (Figure

4-7B). When the data are compared to the trends that would be expected for

both a Rayleigh fractionation model (where the reaction product is isolated from

further isotopic exchange with the system after formation) and a closed-system

equilibrium model (where the reaction components remain open to isotopic

exchange throughout the duration of the reaction), we find that our data fall in

between. Finally, isotopic mass-balance between Fe(II)$_{aq}$ and the solid

precipitate is attained in all cases for solid-liquid pairs early in the experiments

(where the true fractionations are best constrained) within the 2σ error of the

isotopic measurements and calculated F values. The exception to this is the

Thiodictyon strain F4 culture at 120 cm light distance. In this experiment, the

δ^{56}Fe values of Fe(II)$_{aq}$ change between days 2 and 12, despite no significant

change in Fe(II)$_{aq}$ contents, resulting in an F value of zero (Table 4-3). This

observation suggests that small amounts of precipitate were forming early in the

experiment that were below our detection limit.
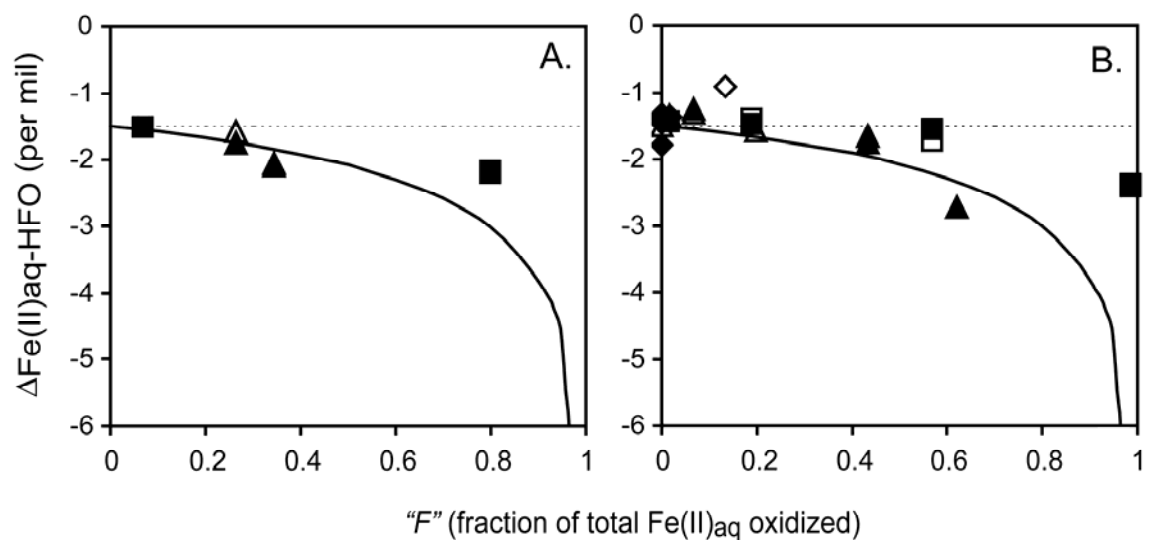
Figure 4-7: Fe isotope fractionations between Fe(II)$_{aq}$ and HFO in the

enrichments and *Thiodictyon* strain F4 cultures. $\Delta_{Fe(II)aq\text{-}HFO}$ values are plotted as

a function of "*F*", defined as the fraction toward complete oxidation of initial

Fe(II)$_{aq}$. Note that the true isotopic fractionation factor (assuming it is constant

over the reaction progress) is most closely constrained at low "*F*" values. Open

and closed symbols of the same type represent the difference between the δ^{56}Fe

values of Fe(II)$_{aq}$ and HFO samplings, in duplicate, for a particular culture. A.

The enrichments. ■ and □ - enrichment 1. ▲ and △ - enrichment 2. B.

Thiodictyon strain F4. ■ and □ - the 40 cm culture. ▲ and △ - the 80 cm

culture. ◆ and ◇- the 120 cm culture. Rayleigh (solid curved line) and closed-

system (dashed straight line) equilibrium models are shown for comparison.

Table 4-4: Summary of fractionation factors using initial precipitates. Errors for

individual experiments based on 1-standard deviation of the duplicate aliquots.

Error for the Grand Average is based on the square root of the sum of the

squares of the errors for the individual experiments.

Experiment	$\Delta_{\textbf{Fe(II)-HFO}}$
Enrichment 1 (Day 9)	-1.59 ± 0.15 ‰ (1σ)
Enrichment 2 (Day 9)	-1.68 ± 0.09 ‰ (1σ)
Thiodictyon strain F4, 40 cm, light (Day 4)	-1.46 ± 0.07 ‰ (1σ)
Thiodictyon strain F4, 80 cm, light (Day 6)	-1.60 ± 0.13 ‰ (1σ)
Thiodictyon strain F4, 120 cm, light (Day 6)	-1.39 ± 0.07 ‰ (1σ)
Grand Average	**-1.54 ± 0.24 ‰ (1σ)**

It is surprising that our data do not follow a Rayleigh fractionation model

because the product of Fe(II)-oxidation is a ferric (hydr)oxide solid that is not

expected to significantly exchange with the fluid after formation. Isotopic

exchange experiments using enriched ^{57}Fe tracers have shown that although

there is isotopic exchange between aqueous Fe and three nanometer (nm)

particles of ferrihydrite, this exchange is dominated by interaction with surface sites over timescales of days to weeks [133]. While it is difficult to measure the particle size of the culture precipitates because they aggregate, we may approximate their individual diameters as between 2-25 nm based on studies of natural and synthetic 2-line ferrihydrite [151]. Given the potentially high surface-to-volume ratio of these particles, isotopic exchange between aqueous Fe and ferrihydrite surface sites may have contributed to the difference between our measured values and the Rayleigh model. It is also possible that small nanoparticles of HFO passed through the filter during sample processing, and thus could have decreased the magnitude of the measured $\Delta_{Fe(II)-HFO}$ fractionation. This effect would be very small at the beginning of the reaction, when $Fe(II)_{aq}$ contents were high, but could become pronounced toward the end of the experiments where $Fe(II)_{aq}$ contents were low.

There are a number of steps in which Fe isotope fractionation could be occurring in our experimental system. First, isotopic fractionation could occur during binding of Fe(II) from the medium to a receptor ligand on or in the cell. Fractionation may also occur in a second step, during oxidation of the biologically bound Fe(II) to an aqueous Fe(III) species. Third, isotopic fractionation may occur between free or cell-associated Fe(II) and Fe(III) species. Fourth, precipitation of HFO might fractionate Fe, as might adsorption of Fe(II) onto HFO and/or cell surfaces. Finally, isotopic exchange between aqueous Fe and the HFO product might contribute. For each of these possibilities, isotopic fractionations may occur through kinetic or equilibrium processes.

Isotopic fractionation mechanisms: possible abiotic mechanisms

The approximately -1.5‰ fractionation between $Fe(II)_{aq}$ and HFO measured in our photosynthetic Fe(II)-oxidizing experiments is similar to that obtained in an abiotic system studied by Bullen et al. (2001). In these experiments, an $Fe(II)Cl_2$ solution was oxidized to ferrihydrite by raising the pH through the addition of $NaHCO_3$. Bullen et al. (2001) interpreted their measured Fe isotope fractionations to reflect isotopic exchange between $Fe(II)_{aq}$ and $Fe(II)(OH)X_{(aq)}$ species, noting that $Fe(II)(OH)X_{(aq)}$ is the most reactive species, and therefore an important precursor to ferrihydrite. While similar reactions might have occurred in our experiments, two major differences between the present study and that of Bullen et al. (2001) are 1.) that the later was performed under aerobic conditions, whereas our study was performed strictly anaerobically, and 2.) that the overall oxidation and precipitation rates of the Bullen et al. (2001) experiment were $\sim 10^3$ times faster than those used in our study. Although the final fractionation factor measured by Bullen et al. (2001) is indistinguishable from that measured early in our experiments (Table 4-4), the initial fractionation factor (-0.9±0.2‰) measured by Bullen et al. (2001) is significantly different. This makes it difficult to conclude that the fractionation factors observed in the two experiments result entirely from a common mechanism.

Despite these differences, a kinetic isotope effect during precipitation may have partially contributed to the fractionations measured in this study and that of Bullen et al. (2001). Drawing upon analogy with the study of Fe(III)-hematite fractionations by Skulan et al. (2002), who observed that kinetic $\Delta_{Fe(III)-Hematite}$

fractionations increased with increasing precipitation rates, we would expect rapid precipitation to produce significant Fe(III)-HFO fractionations (provided that the precipitation is not quantitative; [173]). Although we were able to control the rate of biological Fe(II)-oxidation in our experiments, which limited the overall precipitation rate by controlling the amount of Fe(III) available for precipitation, we were unable to control the rate at which aqueous Fe(III) converted to HFO. If, for example, a kinetic isotopic fractionation existed between Fe(III) and HFO in our experiments, and the $\Delta_{Fe(III)-HFO}$ kinetic fractionation is positive, then the measured $\Delta_{Fe(III)-HFO}$ fractionations would be smaller than those that truly existed between aqueous Fe(III) and Fe(II) pools in our experiments.

One final abiotic Fe isotope fractionation mechanism that may be common to our experiments and those of others, is that associated with Fe(II) sorption onto Fe (hydr)oxide minerals [75]. Assuming an HFO surface area of 600 m^2/g and a sorption capacity of 3 x 10^{-6} mol Fe(II)/m^2 [140], we calculate that only a small amount (<1%) of Fe(II) could have sorbed to HFO during early stages in the reaction progress. A surface area of 600 m^2/g is probably a maximum value, and if the HFO precipitates in our experiments consisted of larger crystals, or were highly clumped, the effective surface area would be much smaller. Nevertheless, even assuming a high surface area, we would not expect sorption to affect the isotopic composition of the system unless the fractionation during sorption was many 10's of per mil or greater, which seems unlikely.

Isotopic fractionation mechanisms: possible biological mechanisms

Identifying a biological mechanism for producing Fe isotope fractionation by Fe(II)-oxidizing phototrophs is challenging due to our lack of understanding of how these bacteria oxidize Fe(II) at the molecular level. For example, it is not yet clear whether oxidation of Fe(II) occurs inside or outside the cell. It has been proposed that oxidation of Fe(II) occurs at the cell surface and that electrons are shuttled to the phototrophic reaction center within the cytoplasmic membrane via a periplasmic transport system [52]. Alternatively, Fe(II) may be oxidized intracellularly by an enzyme located in the periplasm, as is the case for photoautotrophic sulfide oxidation by the sulfide-quinone reductase of Rhodobacter capsulatus [150]. If Fe(II) is oxidized intracellularly, we might expect that cell-produced Fe-chelators would help prevent intracellular precipitation of Fe(III) and/or mediate the export of Fe out of the cell. Alternatively, it is possible that Fe(III) is coordinated by inorganic ligands and that subtle changes in local pH control Fe(III) precipitation. The details of the metabolic steps involved in biological Fe(II)-oxidation may have significant implications for our interpretation of the Fe isotope fractionations produced by these bacteria, and a priority for future work is to elucidate the oxidation pathway.

Despite these uncertainties, our results suggest that equilibrium exchange between biological ligands is a possible explanation for the measured iron isotope fractionation. Although both theoretical and experimental work suggest that there are ligands that preferentially bind Fe(II) with strong covalent bonds [117, 132, 146], it seems more likely that the observed Fe isotope fractionations

are due to isotopic exchange between Fe(II) and Fe(III) species, given that some of the largest Fe isotope fractionations are predicted to occur between ferric and ferrous species [86, 132, 146, 181]. While we cannot be certain that our system was in isotopic equilibrium, it is striking (although perhaps coincidental) that different strains of the Fe(III)-reducing species *Shewanella alga*, grown using ferrihydrite or hematite as an electron acceptor, produce an approximately -1.3 ‰ fractionation in ^{56}Fe /^{54}Fe ratios between Fe(II) and ferric (hydr)oxide substrates [10, 11]. This isotopic fractionation is similar to the Fe isotope fractionations measured in this study, despite the fact that the phototrophic and *S. alga* cultures convert Fe via different redox reaction pathways, and at different rates.

If isotopic exchange between Fe(II) and Fe(III) is an important mechanism for the fractionation observed in the Fe(II)-oxidizing and Fe(III)-reducing biological experiments, this would seem to require ligands with similar binding strengths to be present in both systems. Whether these ligands are present as free species or cell-associated (*i.e.*, bound to a protein or a cell surface polymer) is unknown. However, given the abundance of Fe(II) in our experiments, it seems unlikely that Fe(II) would be chelated by a free biological ligand. Although we could not measure an aqueous pool of Fe(III) in our experiments, it is possible that the exchangeable Fe(III) pool is very small and below the detection limit of our assay. The characterization of Fe binding ligands (be they in solution or cell-associated) in both Fe(II)-oxidizing and Fe(III)-reducing biological systems is a necessary next step to better understand Fe isotope fractionation.

CONCLUSIONS

Iron isotope fractionation produced by diverse Fe(II)-oxidizing anaerobic phototropic bacteria results in poorly crystalline HFO products that have ^{56}Fe /^{54}Fe ratios that are ~1.5±0.2‰ higher than the Fe(II)$_{aq}$ electron donor. The measured isotope fractionations appear to be independent of the overall rate of Fe(II)-oxidation. Equilibrium isotope exchange between Fe(II) and Fe(III) bound to biological ligands may explain the observed fractionation. Alternatively, a kinetic isotope effect of rapid HFO precipitation overlying an equilibrium effect produced by ligand exchange is also consistent with the data. Despite a number of uncertainties in the mechanisms that underlie the observed isotopic fractionations, these results show that photosynthetic Fe(II)-oxidation, under anaerobic conditions, will produce ferric (hydr)oxide precipitates that have high δ^{56}Fe values relative to Fe(II)$_{aq}$ sources.

Can an Fe isotope "fingerprint" of anaerobic photosynthetic Fe(II)-oxidizing bacteria be recognized in the rock record? Johnson et al. (2003) noted that the moderately positive δ^{56}Fe values found in some oxide layers of the 2.5 Ga Kuruman and Griquatown Iron Formations might be explained by the +1.5‰ HFO-Fe(II)$_{aq}$ fractionations produced by Fe(II)-oxidizing phototrophs, assuming that ancient Fe(II) sources had moderately negative δ^{56}Fe values (~ -0.5‰), such as those of modern mid-ocean ridge hydrothermal fluids [12, 152]. If ambient oxygen contents were low at 2.5 Ga, as has been argued by many workers [58, 74, 91, 145], photoautotrophic Fe(II)-oxidizing bacteria may indeed be the best explanation for the occurrence of ferric oxides that have high δ^{56}Fe values in the

Archean rock record. It is as yet unknown what the Fe isotope effects would be of UV-photo-oxidation, which is an alternative means for producing ferric oxides in an anoxic environment [24]. If, however, ambient oxygen levels were sufficiently high in the Archean that oxidation of Fe(II) by oxygen could have occurred, similarly high δ^{56}Fe values for ferric oxides may have been produced. It therefore seems likely that interpretation of the Fe isotope record in terms of oxidative processes will require independent evidence regarding ambient oxygen contents in a particular environment.